

[Click here to view linked References](#)

## Site response analyses for complex geological and morphological conditions: relevant case-histories from 3<sup>rd</sup> level seismic microzonation in Central Italy

Pagliaroli A.<sup>1</sup>, Pergalani F.<sup>2</sup>, Ciancimino A.<sup>3</sup>, Chiaradonna A.<sup>4</sup>, Compagnoni M.<sup>2</sup>, de Silva F.<sup>4</sup>, Foti S.<sup>3</sup>, Giallini S.<sup>1,5</sup>, Lanzo G.<sup>6</sup>, Lombardi F.<sup>2</sup>, Luzi L.<sup>7</sup>, Macerola L.<sup>8</sup>, Nocentini M.<sup>5</sup>, Pizzi A.<sup>8</sup>, Tallini M.<sup>8</sup>, Teramo C.<sup>9</sup>

<sup>1</sup> Università degli Studi *G. d'Annunzio*, Chieti-Pescara, Italy

<sup>2</sup> Politecnico di Milano, Italy

<sup>3</sup> Politecnico di Torino, Italy

<sup>4</sup> Università degli Studi di Napoli *Federico II*, Istituto di Geologia Ambientale e Geoingegneria (IGAG), CNR, Roma, Italy

<sup>5</sup> Istituto di Geologia Ambientale e Geoingegneria (IGAG), CNR, Roma, Italy

<sup>6</sup> *Sapienza* Università di Roma, Italy

<sup>7</sup> Istituto Nazionale di Geofisica e Vulcanologia (INGV), Milano

<sup>8</sup> Università degli Studi dell'Aquila, Italy

<sup>9</sup> Engineer, Messina, Italy

Corresponding Author: [alessandro.pagliaroli@unich.it](mailto:alessandro.pagliaroli@unich.it)

### Abstract

The paper presents the results of 5 case studies on complex site effects selected within the project for the level 3 seismic microzonation of several municipalities of Central Italy damaged by the 2016 seismic sequence. The case **studies** are characterized by different geological and morphological **configurations**: Monte San Martino is located along a hill slope, Montedinove and Arquata del Tronto villages are located at ridge top whereas Capitignano and Norcia lie in correspondence of sediment-filled valleys. Peculiarities of the sites are constituted by the presence of weathered/jointed rock mass, fault zone, shear wave velocity inversion, complex surface and buried morphologies. These factors make the definition of the subsoil model and the evaluation of the local response particularly complex and difficult to ascertain. For each site, after the discussion of the subsoil model, the results of site response numerical analyses are presented in terms of amplification factors and acceleration response spectra in selected points. The physical phenomena governing the site response have also been investigated at each site by comparing 1D and 2D numerical analyses. Implications are deduced **for seismic microzonation studies** in similar geological and morphological conditions.

### Keywords

Seismic microzonation, Amplification factors, Response spectra, Numerical analyses, Complex geological and morphological conditions

## 1. Introduction

Seismic Microzonation studies of level 3 (i.e., according to Working Group ICMS 2008 studies based on quantitative assessment of site effects by means of numerical analyses) were carried out for the reconstruction of several municipalities in Central Italy struck by the 2016 seismic events. The sequence started with the Mw 6.0 earthquake on August 24, 2016, followed by the Mw 5.9 on 26 October and the Mw 6.5 on 30 October events (Chiaraluce et al., 2017). The studies were executed by professionals (mainly geologist and geotechnical engineers) with the scientific supervision and support of the Center for Seismic Microzonation and its applications (*CentroMS*, <https://www.centromicrozonazioneismica.it/en/>) constituted by several university departments and research institutes. In particular, the *CentroMS* has taken care of some activities in all the municipalities: i) definition of the input motion at rock outcrop; ii) experimental characterization of nonlinear soil behavior by means of cyclic/dynamic laboratory tests; iii) execution of bidimensional site response analyses.

In the paper, the results of the numerical analyses carried out in 5 selected sites characterized by different morphological and geological conditions are reported. Specifically, as indicated in Figure 1, three sites are located in Marche region (Arquata del Tronto, Monte San Martino, and Montedinove), one in Abruzzo (Capitignano) and the other one in Umbria region (Norcia). The main features encountered in the selected sites are briefly summarized hereafter:

- 1) Monte San Martino lies on a structurally asymmetric gentle hill characterized by an outcropping seismic bedrock on one side and soft eluvio-colluvial covers on the other flank;
- 2) Arquata del Tronto is located on the top of a ridge characterized by the alternation of different rocky lithotypes, weathered and jointed in the upper portion;
- 3) Montedinove site represents a symmetrical ridge situation characterized by the presence of an inversion in the shear wave velocity ( $V_s$ ) profile;
- 4) Capitignano lies close to a complex fault zone at the NE edge of a sediment-filled deep valley with maximum thickness up to 200 m;
- 5) Norcia is in the middle of a “shallow” large intermontane basin with the presence of inversion of shear wave velocity with depth.

In the framework of the seismic microzonation project, in all sites, in situ tests were carried out comprising down-hole (DH), Multichannel Analysis of Surface Waves (MASW), and Horizontal to Vertical Spectral Ratios (HVSr) tests (Caielli et al., 2019 this issue). In some sites, other in situ tests were also available from previous microzonation studies such as Electrical Resistivity Tomography (ERT), P-wave seismic refraction (SR), Refraction Microtremor (REMI) and Extended Spatial Autocorrelation (ESAC) passive tests. On sites where it was possible to retrieve undisturbed soil samples, resonant column (RC)/torsional shear (TS) tests were also carried out. An overview of the geotechnical characterization of nonlinear soil behaviour is reported in Ciancimino et al. 2019 (this issue).

The 1D numerical analyses have been performed using STRATA (Kottke and Rathje, 2008) or Deepsoil 6.1 (Hashash et al., 2016), operating in the frequency domain, and using the equivalent-linear visco-elastic approach to model cyclic soil behaviour. The 2D analyses were carried out through the time domain 2D FEM codes LSR2D (Stacec 2017, Macerola 2017) for Montedinove and Capitignano case studies, and QUAD4M (Hudson et al., 1994), for Monte San Martino, Arquata del Tronto and Norcia. Both 2D codes adopt an equivalent-linear visco-elastic approach and incorporate a compliant base. The side boundaries were modelled as perfectly reflecting and thus they were extended 200-400 m in both directions to reduce the influence of artificial reflected waves. The mesh was defined by means of triangular/quadrangular elements with a size consistent with the shear wave velocity of each lithotype, so as to ensure an accurate wave propagation up to a maximum frequency of 15-20 Hz depending on case study (Kuhlemeyer and Lysmer, 1973). Viscous damping was introduced through full Rayleigh damping formulation with two control frequencies automatically selected by the codes in order to avoid significant overdamping in all the frequency range of interest (Lanzo et al., 2003). Preliminary calibration analyses showed that the 2D codes give comparable results (Di Buccio et al., 2017). Further details on these codes and their use in level 3 microzonation studies can be found in Pagliaroli (2018).

In all sites the input motions consisted of seven unscaled horizontal natural records, selected by the ITACA archive ([itaca.mi.ingv.it/](http://itaca.mi.ingv.it/), Luzi et al. 2008) to be compatible on average in the 0.1-1.1s period range with the Uniform Hazard Spectrum (return period  $T_R = 475$  yrs) at rock conditions (subsoil class A) as proposed by the Italian Building Code (NTC2018). The accelerograms used as input motion are listed in Table 1 for each site. For each record, the following characteristics are presented: earthquake data and name, moment magnitude, epicentral distance, name and code of the recording station and corresponding subsoil classification according Eurocode 8-NTC2018, horizontal component used. The corresponding 5% damped response spectra are presented in Figure 2 together with the comparison between the average input spectrum and the reference NTC2018 shape. More details on the procedure followed for the definition of input motion are reported in Luzi et al. 2019a (this issue).

Results of numerical analyses are generally presented in terms of elastic acceleration response spectra ( $S_e$ ) and amplification factors of spectral acceleration (AF). These latter are defined as the ratio between the elastic average

response spectra at the ground surface and the corresponding input motion response spectra **integrated over** three period ranges 0.1-0.5s, 0.4-0.8s and 0.7-1.1s, labelled  $AF_{0.1-0.5}$ ,  $AF_{0.4-0.8}$  and  $AF_{0.7-1.1}$  respectively. In the following, for each case study the main morphological and geological features, the subsoil model and the results of the numerical analyses are summarized. The geological features are represented in terms of lithotechnical map and cross-sections in which the different lithotypes are identified according to Italian standard for Microzonation (Bramerini et al., 2015). The attention is focused on the analysis of the physical phenomena responsible for ground motion amplification in such complex sites. Moreover, critical issues in defining the subsoil model are highlighted. Lessons learned for advanced seismic microzonation studies are addressed in the conclusions.

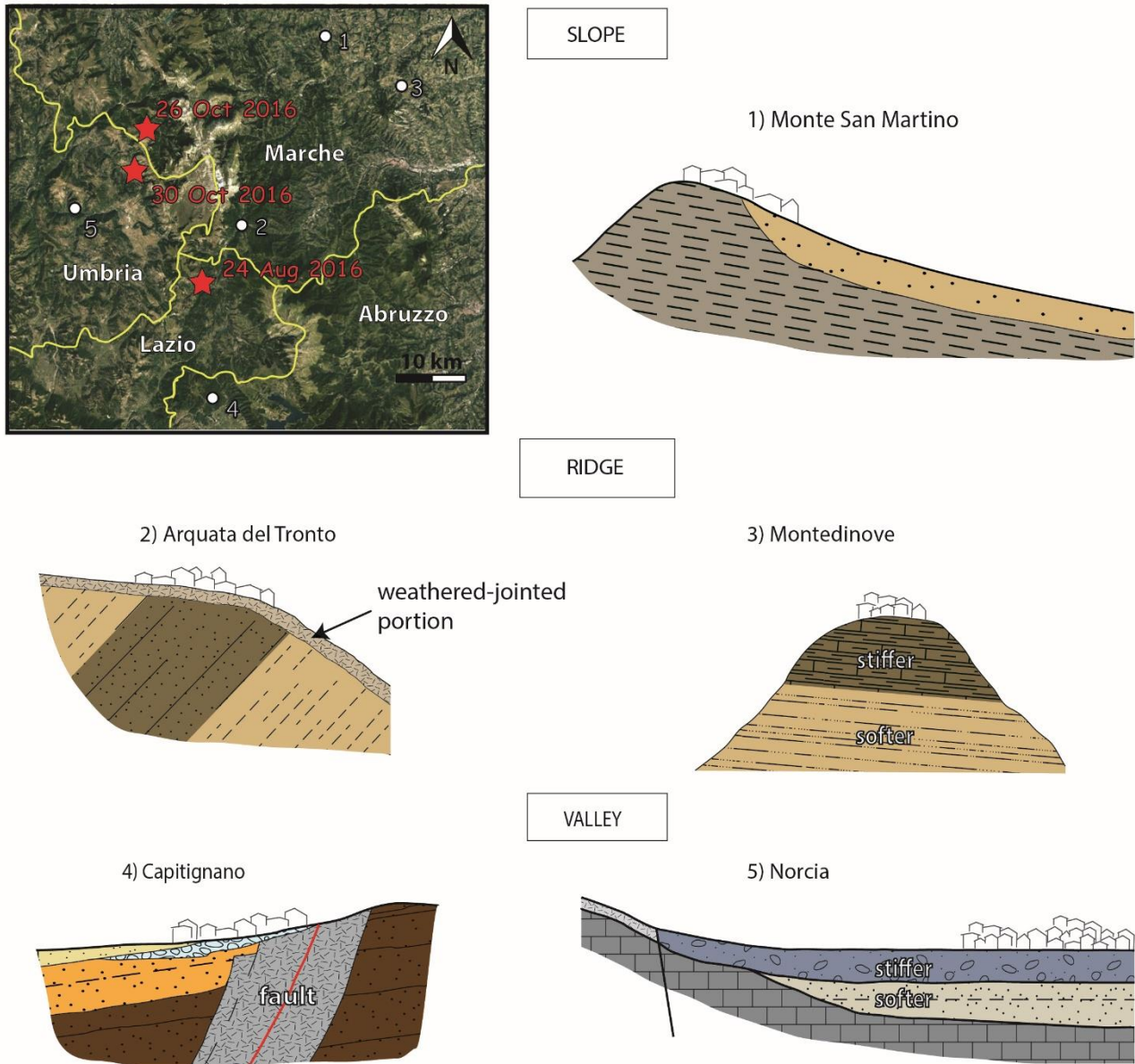


Figure 1. Selected sites presented in the paper and sketch of the corresponding geological/morphological configurations.

*Table 1 - Characteristics of natural accelerograms selected as input motion for the five sites presented in the paper (A\* = subsoil category A attributed based on available geological information at recording station)*

Site	Acc.	Event	Date	Mw	Epic. Distance (km)	Station (code-name)	Comp.	Site class. EC8
Monte San Martino	#1	Central Italy	30.10.2016	6.5	24.8	MZ11-bedrock nord Sant'Angelo	EW	A*
	#2	Central Italy	30.10.2016	6.5	22.6	MZ19-Pasciano cimitero	NS	A*
	#3	Central Italy	26.10.2016	5.9	10.8	CLO-Castelluccio di Norcia	EW	A*
	#4	Central Italy	26.10.2016	5.9	10.8	CLO-Castelluccio di Norcia	NS	A*
	#5	Central Italy	30.10.2016	6.5	19.2	MMO-Montemonaco	EW	A*
	#6	Central Italy	30.10.2016	6.5	19.2	MMO-Montemonaco	NS	A*
	#7	Central Italy	26.10.2016	5.4	15.8	T1212-Avendita PG	EW	A*
Arquata del Tronto	#1	Central Italy	30.10.2016	6.5	27.7	MZ10-Amatrice	NS	A*
	#2	Central Italy	26.10.2016	5.4	27.9	MZ21-Poggio Vitellino	EW	A*
	#3	Central Italy	30.10.2016	6.5	18.6	ACC- Accumuli	NS	A*
	#4	Central Italy	26.10.2016	5.9	10.8	CLO- Castelluccio di Norcia	EW	A*
	#5	Central Italy	26.10.2016	5.9	10.8	CLO- Castelluccio di Norcia	NS	A*
	#6	Central Italy	30.10.2016	6.5	19.2	MMO-Montemonaco	NS	A*
	#7	Central Italy	30.10.2016	6.5	10.5	T1212-Avendita PG	NS	A*
Montedinove	#1	Central Italy	30.10.2016	6.5	24.5	MZ11-bedrock nord Sant'Angelo	EW	A*
	#2	Central Italy	30.10.2016	6.5	22.6	MZ19 - Pasciano cimitero	NS	A*
	#3	Central Italy	26.10.2016	5.9	10.8	CLO - Castelluccio di Norcia	EW	A*
	#4	Central Italy	26.10.2016	5.9	10.8	CLO - Castelluccio di Norcia	NS	A*
	#5	Central Italy	30.10.2016	6.5	19.2	MMO - Montemonaco	EW	A*
	#6	Central Italy	30.10.2016	6.5	19.2	MMO - Montemonaco	NS	A*
	#7	Central Italy	26.10.2016	5.4	15.8	T1212 - Avendita PG	EW	A*
Capitignano	#1	Central Italy	30.10.2016	6.5	22.6	MZ19-Pasciano cimitero	HNE	A*
	#2	Central Italy	30.10.2016	6.5	22.6	MZ19-Pasciano cimitero	HNN	A*
	#3	Central Italy	30.10.2016	6.5	18.6	ACC-Accumoli	HGE	A*
	#4	Central Italy	26.01.2016	5.9	10.8	CLO-Castelluccio di Norcia	HGE	A*
	#5	Central Italy	26.01.2016	5.9	10.8	CLO-Castelluccio di Norcia	HGN	A*
	#6	Central Italy	30.10.2016	6.5	19.2	MMO-Monte monaco	HGN	A*
	#7	Central Italy	30.10.2016	6.5	10.5	T1212-Avendita PG	HNN	A*
Norcia	#1	Central Italy	30.10.2016	6.5	22.6	MZ19-Pasciano Cimitero	EW	A*
	#2	Central Italy	30.10.2016	6.5	22.6	MZ19-Pasciano Cimitero	NS	A*
	#3	Central Italy	30.10.2016	6.5	18.6	ACC-Accumuli	EW	A*
	#4	Central Italy	26.10.2016	5.9	10.8	CLO-Castelluccio di Norcia	EW	A*
	#5	Central Italy	26.10.2016	5.9	10.8	CLO-Castelluccio di Norcia	NS	A*
	#6	Central Italy	30.10.2016	6.5	19.2	MMO-Montemonaco	NS	A*
	#7	Central Italy	30.10.2016	6.5	10.5	T1212-Avendita PG	NS	A*

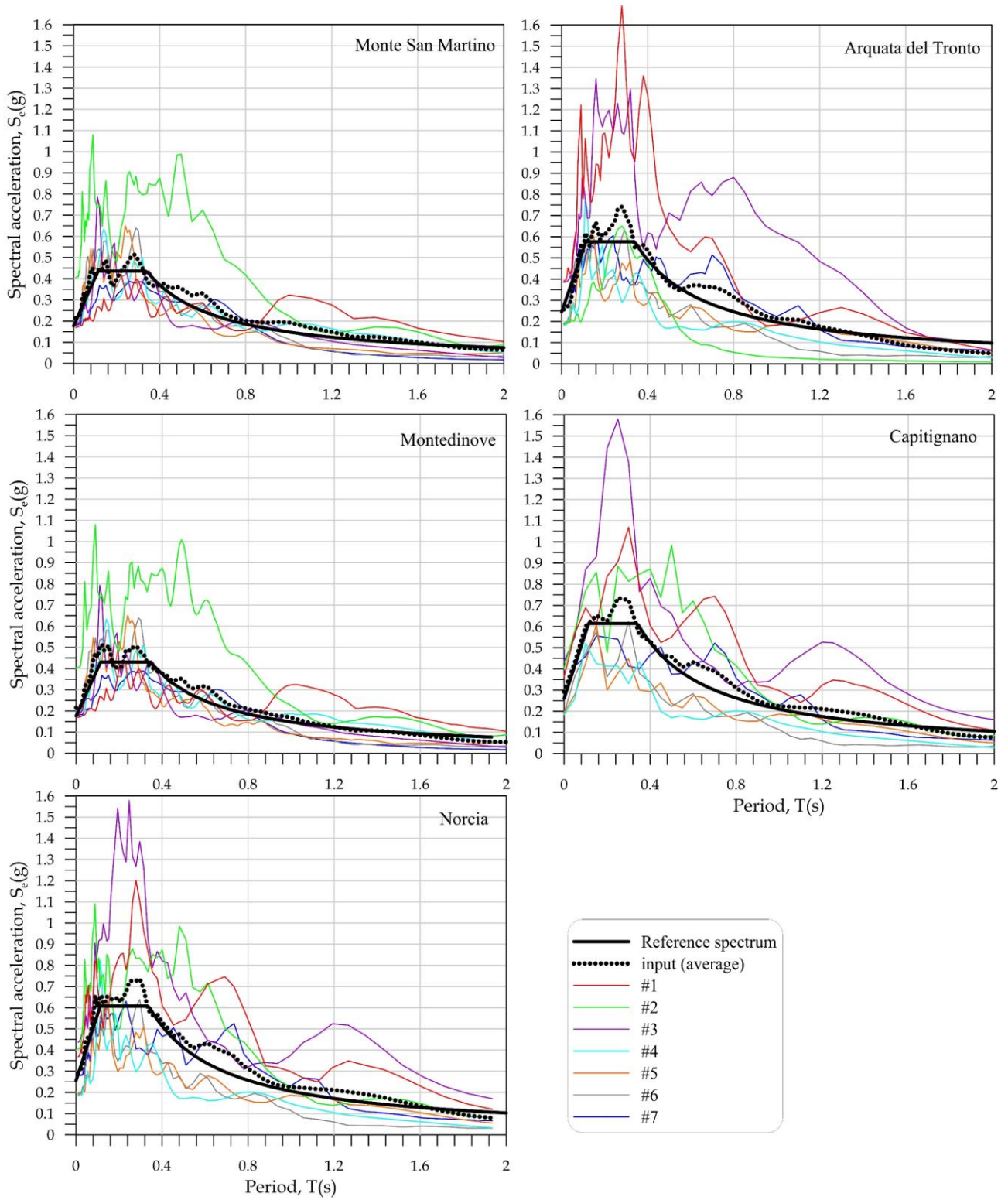


Figure 2 – Response spectra of the 7 accelerograms selected as input motion for each of the five sites discussed in the paper (see Table 1 for the list of signals); the comparison between the average spectrum with the reference one is also reported.

## 2. Monte San Martino site

### 2.1 Morphological and geological outlines

Monte San Martino is a small village in the Marche region, located about 30 km south of Macerata. The city centre lies on a rocky hill at 603 m a.s.l. between two deep valleys that separate Monte San Martino from the neighbouring municipalities located on the top of the surrounding hills.

Figure 3a shows the lithotechnical map of the area, with location of in-situ investigations and the trace of a representative cross-section oriented in the WSW-ENE direction. The related cross-section is reported in Figure 3b, in which several lithotechnical and geological units can be identified.

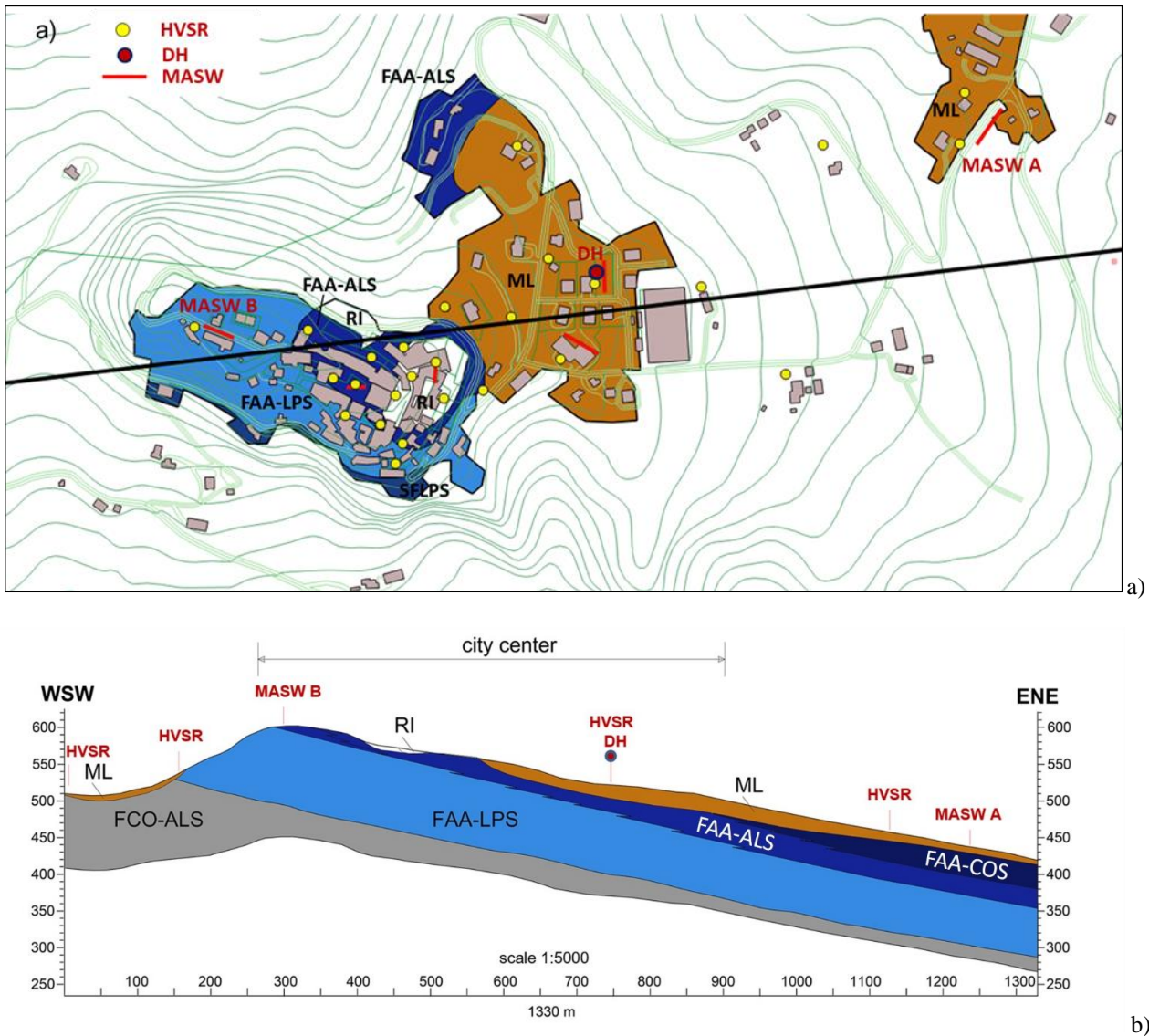


Figure 3. Monte San Martino lithotechnical map (a) and analysed cross-section (b); *geologic unit abbreviations in the text.*

In the studied area, the Blue Clays Formation (*Formazione delle Argille Azzurre*: FAA in Figure 3) widely outcrops. This formation can be subdivided in three different lithotypes, consisting of (Regione Marche, 2001): 1 - mainly arenaceous lithofacies, i.e. alternations of thick arenaceous layers, locally cemented, and thin pelitic layers (1- 3cm), largely outcropping in the study area; 2 - arenaceous-pelitic lithofacies with sand/clay ratio higher than one, characterized by alternations of arenaceous and pelitic layers between 30 and 50 cm thick; 3 - blue clay with interleaved sandy horizons. These different lithotypes, following the standard for microzonation, are identified as LPS (layered rocky lithotype), ALS (alternation of stratified lithotypes), and COS (cohesive, overconsolidated stratified bedrock),

respectively. Below the blue clays Formation, the geological bedrock is made of pelitic-arenaceous lithofacies with sand/clay ratio lower than one, recognized as “Colombacci” Formation (FCO-ALS in Figure 3b) (Regione Marche, 2001).

Eluvio-colluvial deposits (ML in Figure 3), constituted by clayey silt and silty sand, locally including arenaceous clasts, cover FFA in the eastern flank. Finally, on the top of the hill, a landfill material in a silty-sandy matrix (RI) has been recognized.

## 2.2 Subsoil model

The seismic response analyses of Monte San Martino were performed on the numerical model plotted in Figure 4a, reproducing the WSW-ENE geological section (Figure 3b). The DH and MASW tests performed during the microzonation study are reported together with the main frequencies derived from the interpretation of ambient noise records through the HVSR technique. Table 2 summarizes the physical and mechanical properties assigned to the layers.

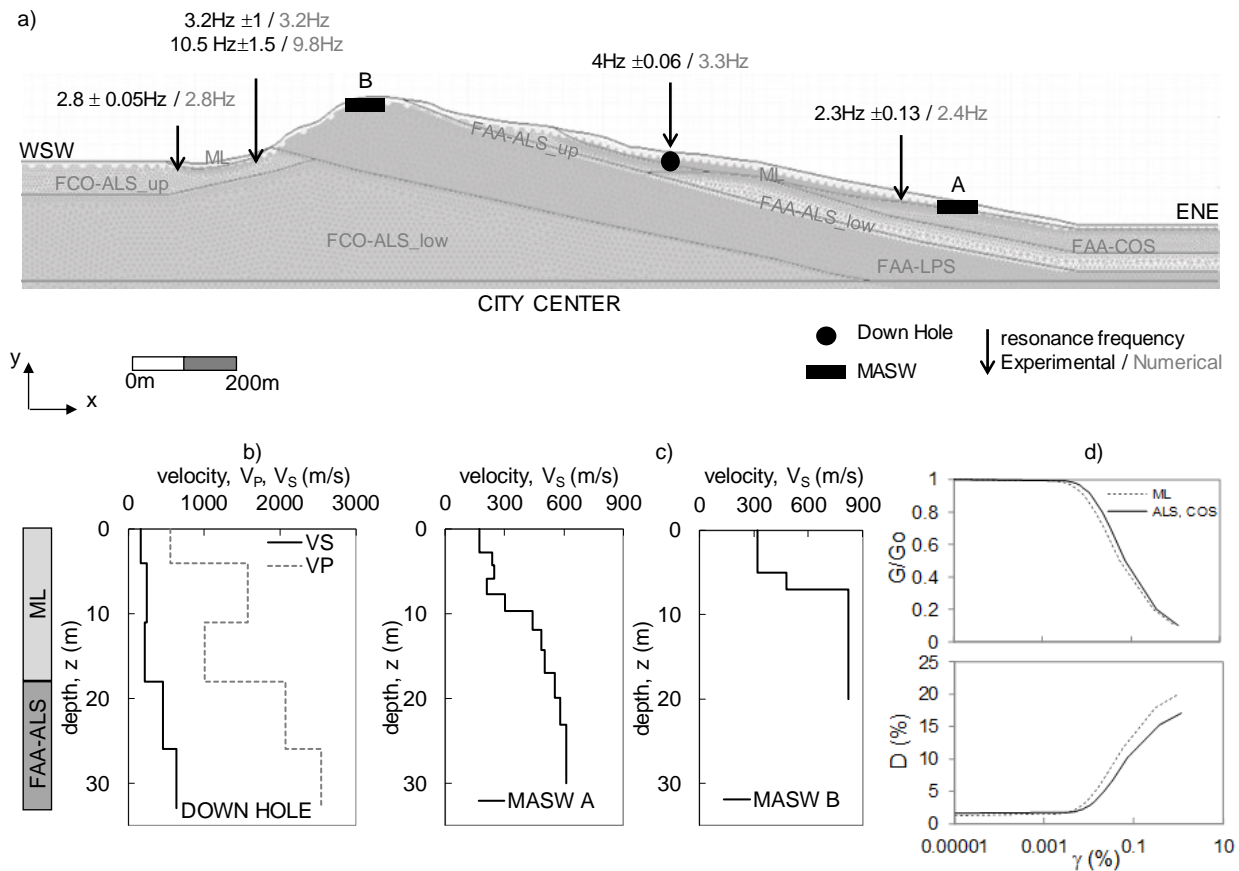


Figure 4. *Monte San Martino site*: results of relevant testing for the definition of subsoil model (a),  $V_P$  and  $V_S$  profiles measured through the down hole test in the ML and FAA-ALS lithotypes (b),  $V_S$  profiles inferred from the MASW A and B tests (c) and  $G/G_0-\gamma$  and  $D-\gamma$  curves resulting from the RC-TS tests (d); black and grey number along the cross-section in the upper portion represent experimental and numerical estimation of first natural frequency respectively.

The compression,  $V_P$ , and the shear,  $V_S$ , wave velocities of the ML and FAA-ALS deposits were measured through the DH test until the depth of 33 m reached by the borehole (see Figure 4b), while the  $V_S$  profiles of the FAA-COS and FAA-LPS layers derive from the results of MASW A and MASW B tests respectively, shown in Figure 4c. The mean value of the slightly variable  $V_P$  and  $V_S$  profiles were assigned to the ML material model, while an upper and softer sublayer, FAA-ALS up, was distinguished in the blue-grey clay deposit, according to the down-hole measurements. The mean  $V_S$  was set for the FAA-COS soil, again due to the low variability. The FAA-LPS formation was assumed as bedrock ( $V_S=800\text{m/s}$ ), neglecting the lower shear wave velocity detected in the surface and attributable to local jointed/weathered portions.

Because of insufficient investigations, the  $V_s$  of the FCO-ALS deposit was inferred from MASW tests performed at Carassai site, 35 km far from Monte San Martino, and the bedrock depth was calibrated to obtain the resonant frequencies measured on site through the HVSr tests.

The Poisson's ratio of the FAA-COS, FAA-LPS and FCO-ALS deposits were assumed considering data on similar formations investigated in Central Italy towns subjected to microzonation studies.

The low-strain parameters were validated, comparing the experimental predominant frequencies from H/V curves with the resonance frequencies computed through 1D seismic response analyses performed along the same verticals. Figure 4a shows the satisfying agreement between experimental (black) and numerical (grey) values.

An equivalent linear visco-elastic behaviour was assigned to all materials, except for the bedrock. The decay of the shear modulus,  $G$ , and the increase of the damping ratio,  $D$ , with shear strain,  $\gamma$ , was introduced in the numerical model through the curves plotted in Figure 4d. The curves were obtained calibrating the Ramberg-Osgood (1943) model on the results of torsional shear tests (TS in Table 1) on samples of ML and ALS-COS taken in Monte San Martino and in Massa Fermana, respectively. Finally, a linear visco-elastic behaviour was set for the FCO-ALS low and FAA-LPS layers with a constant damping  $D_0=0.5\%$ .

Lithotype	$\gamma$ (kN/m <sup>3</sup> )	$V_s$ (m/s)	$\nu$ (-)	Nonlinear material curves
ML	20.00	220	0.48	TS test Monte San Martino
FAA-COS	22.5	450	0.45	TS test Massa Fermana
FAA-ALS up	22.5	457	0.47	
FAA-ALS low	22.5	630	0.47	
FCO-ALS up	22.5	440	0.45	
FCO-ALS low (bedrock)	22.5	800	0.45	Linear D=0.5%
FAA-LPS (bedrock)	24.00	800	0.45	Linear D=0.5%

Table 2. Monte San Martino site: *selected parameters for subsoil model used for site response analyses*

### 2.3 Numerical modelling: results and discussion

Figure 5 shows the variability along the cross-section surface of the mean amplification factors of the spectral acceleration computed in the period ranges 0.1-0.5s ( $AF_{0.1-0.5s}$ ), 0.4-0.8s ( $AF_{0.4-0.8s}$ ) and 0.7-1.1s ( $AF_{0.7-1.1s}$ ).

The peak amplification factors occur in the range 0.4-0.8 s, slightly higher than the experimental predominant periods reported in Figure 4a in terms of frequencies. The elongation of the resonance periods with respect to the low-strain values measured on site is due to the reduction of shear stiffness associated with the shear strains mobilized under earthquake (i.e., soil nonlinearity). Moreover, the huge scattering of the  $AF_{0.4-0.8s}$  and  $AF_{0.7-1.1s}$  in correspondence with the softest ML layer confirms the expected dependence of AFs on the frequency and amplitude of the input motions. On the other hand, a very low dispersion is associated with the outcropping stiff layers FAA-ALS up and FAA-LPS.

Independently on the period range, the highest AFs occur:

-on the top of the ridge, with peak mean values  $AF_{0.1-0.5s}=1.13$ ,  $AF_{0.4-0.8s}=1.40$  and  $AF_{0.7-1.1s}=1.59$ ;

-on the slope (i.e., eastern flank of the ridge) at the eluvio-colluvial deposit ML, with peak mean values  $AF_{0.1-0.5s}=2.23$ ,  $AF_{0.4-0.8s}=2.50$  and  $AF_{0.7-1.1s}=1.70$ .

To isolate and quantify the stratigraphic amplification, one-dimensional seismic response analyses have been carried out along representative soil columns, identified by verticals V1, V2, V3 and V4 on the cross section in Figure 5. The 1D simulations were performed considering the same soil properties and input motions as 2D response analyses. The results are reported in Figure 5 in terms of mean amplification factors  $AF_{0.1-0.5s}$ ,  $AF_{0.4-0.8s}$  and  $AF_{0.7-1.1s}$ .

With reference to the vertical V1, at the top of the ridge, amplification is exclusively due to topographic effects revealed by 2D analysis; as a matter of fact, 1D amplifications factors are close to 1 in all the period ranges. Nevertheless, considering the moderate slope angles, the amplification factors of 2D analysis can be obtained applying a multiplier of 1.2 to 1.5 to the results of 1D simulations, as suggested by building codes (NTC2018, Eurocode 8).

With reference to the verticals V2, V3 and V4, located on the slope where soil cover outcrops, 1D and 2D computations lead approximately to the same amplification factors. Ground motion amplification is therefore mainly due to



stratigraphic effects which are well-predicted by 1D seismic response analysis and are significantly predominant with respect to 2D effects related to topography and the inclined geometry of the interface between bedrock and soil layers. This result suggests that, in this morphological configuration, one-dimensional seismic response analysis can provide reliable estimation of site effects, despite the presence of an inclined bedrock.

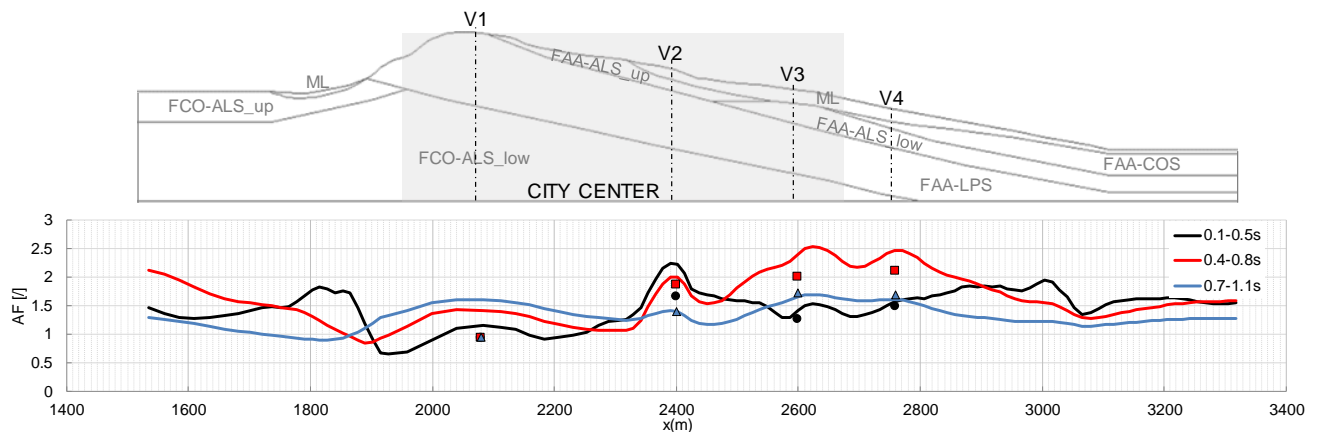


Figure 5. *Monte San Martino site*: variability along the cross-section of the amplification factor in the period range 0.1s-0.5s (a), 0.4s-0.8s (b), 0.7s-1.1s (c) compared to the values computed through 1D seismic response analyses along the verticals V1, V2, V3 and V4

### 3 Arquata del Tronto site

#### 3.1 Morphological and geological outlines

Arquata del Tronto is a municipality located in the central Apennine fold and thrust belt (Central Italy) at the base of the southeastern flank of Mt. Vettore, within the footwall block of the regional, roughly N-S oriented, Sibillini Mts thrust (Neogene) affected by later (Pliocene-Quaternary) NW-SE oriented active normal faults (Koopman, 1986; Pizzi and Galadini, 2009; Pierantoni et al., 2013).

The geological and seismic bedrock is represented by the pre-evaporitic member (Messinian) of the Laga Formation consisting of three turbiditic lithotypes (i.e., lithofacies associations), largely outcropping in the study area, namely in order of the increasing sand/clay ratio (S/C): Arenaceous-pelitic II ( $1 < S/C < 3$ ) (LAG4b in Figure 6), Arenaceous-pelitic I ( $3 < S/C < 10$ ) (LAG4d in Figure 5), Arenaceous ( $S/C >> 1$ ) (LAG4c in Figure 5) (e.g., Centamore et al., 1991; Regione Marche, 2001; Marini et al., 2015)

The village of Arquata is built on an elongated WNW-ESE ridge (730 m a.s.l.) transversally cut by saddles due to the alternation of stiffer/softer lithotypes belonging to the Laga Formation with roughly  $50^\circ$  WNW dipping strata, forming a monocline representing the **overturned** limb of an E-verging anticline (Figure 6).

The ridge rises about 170 m above the Borgo Village lying in the valley located north of Arquata (Figure 6). Here the Laga Formation is locally overlain by Quaternary continental deposits: the fluvial deposits of the Camartina creek and Tronto River (bn1, bn2, and bn3 in Figure 6 for first, second and third order alluvial terraces, respectively) and by detrital (a3a) and landslide (a1a) covers composed of coarse calcareous/arenaceous debris.

On the eastern side of the Pianella Valley, located north-west of the study area (see map in Figure 6), strata of the Laga Formation outcrop dipping  $20^\circ$  towards the east with a  $N5-10^\circ$  trending, and in proximity of the S.Pietro and Paolo Church they tend to approximate a vertical dip. **Such different bedding** of the Laga Formation between the strata outcropping on the right side and left side of the valley is solved by many authors considering the presence of a tectonic structure along the valley: a tear fault, according to Centamore et al. (1991), or a normal fault following Koopman (1986).

A geological cross-section cutting the Arquata del Tronto ridge as drawn by the Istituto Superiore per la Protezione e la Ricerca Ambientale (ISPRA) is reported in Figure 6 showing the stratigraphic relationship between different Laga Formation lithotypes.

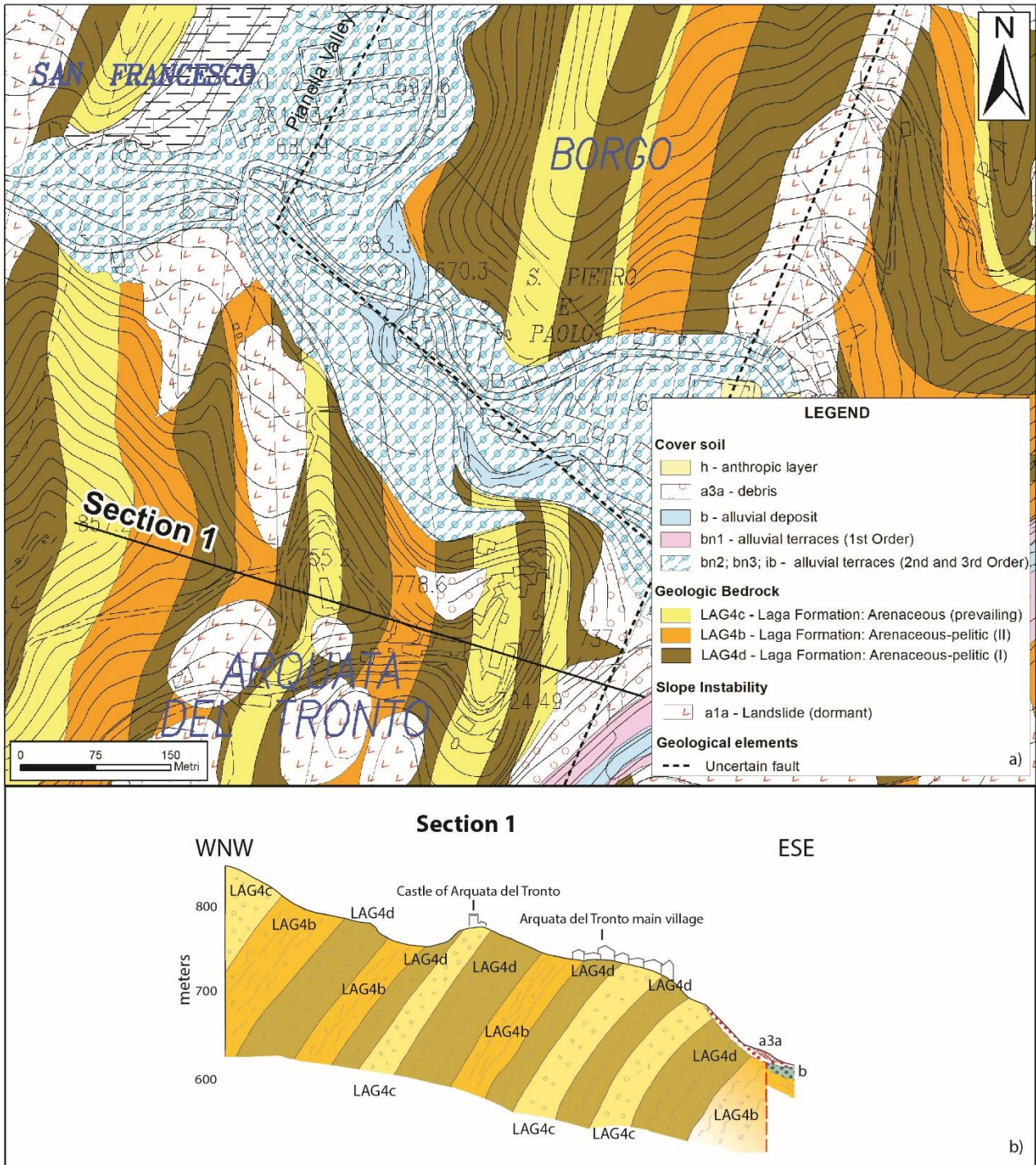
### 3.2 Subsoil model

The mechanical characterization of soils and rocks for the site response analysis of the study area has been achieved consulting the whole geological and geophysical dataset collected in this sector. In particular, the observations derived from the geological field survey have been integrated with DH, MASW, ERT and HVSR tests (location of relevant tests is reported in the map of Figure 7a).

The geological and geophysical investigations carried out in the study area suggest the presence of a weathered/jointed upper portion of the Laga Formation rock mass, approximately 15 meters thick. In Figure 7c two representative DH tests are reported. In detail, the DH5 test carried out on the East side of the Arquata del Tronto ridge flank, on LAG4d outcrop, with the exclusion of the 3-4 meters at surface **consisting of** very highly weathered rock, shows a slight increase with depth of the shear wave velocity ( $V_s$ ) from 750 m/s to 1000 m/s. The upper 15-16m where  $V_s$  is lower than 1000 m/s has been interpreted as the weathered/jointed portion of rock mass. In Figure 7c a DH test (DH\_Ecoscuola) carried out in the San Francesco area, located **North-West** of Arquata del Tronto village, **is also reported**, which intercepted the alluvial cover and reached the seismic bedrock (Laga Formation) at about 30 m depth, where the  $V_s$  attains a value of 1000 m/s. The alluvial cover shows a  $V_s$  increasing with depth from 400 to 700 m/s.

Several HVRS tests were carried out on the Arquata del Tronto ridge, on rock outcrops belonging to different lithotypes. Horizontal-to-vertical spectral ratio has been computed for each measurement, by averaging the H/V ratios obtained on 30-s-long time windows into which each trace (usually 20 to 30 minutes long) was subdivided. The geometrical mean of horizontal components was employed to compute HVSR. Some representative results are reported in Figure 7b for two locations on the ridge: the Arquata del Tronto village (blue box in Figure 7a) and around the Castle (red box). All the measurements highlighted the presence of multiple picks, markers of a possible broad band amplification related to a complex coupling of stratigraphic and topography effects. Polarization analyses (not shown in Figure 7b) have revealed a preferential polarization along N-S direction of the 2-4 Hz peaks in the in the area marked by the blue box (village) while the 1-3 Hz peaks are ENE-WSW oriented around the castle in the NW side of the ridge (red box).

**An interesting observation is that** the H/V curves present higher amplitude peaks if located on stiff arenaceous lithotypes of the Laga Formations as compared to those carried out on pelitic lithotype of the same Formation.



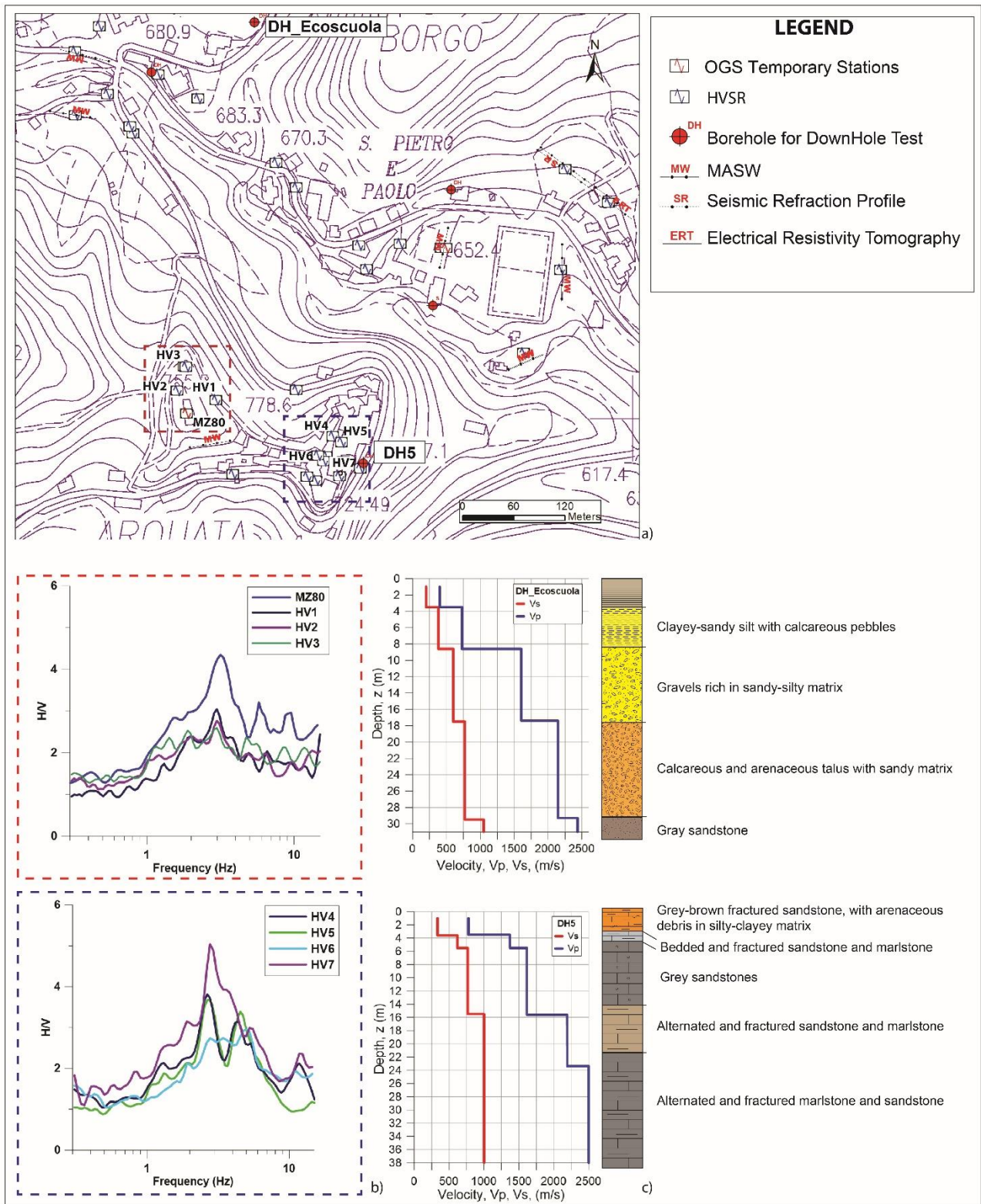


Figure 7. Map of the relevant geophysical and geotechnical investigations in Arquata del Tronto area (a) and representative results in terms of H/V from noise measurements (b) and Vp/Vs profiles from DH tests (c).

The subsoil model adopted for the analyses is reported in Table 3 whereas a sketch of the mesh adopted to discretize section 1 is shown in the upper part of Figure 8. The prevalent arenaceous lithotypes of Laga Formations (LAG4c and

LAG4d) were grouped together and, based on available DH tests, a  $V_s$  of 1000 m/s and 900 m/s was assigned to the arenaceous group and to more pelitic lithotype (LAG4b), respectively. A 15m-thick jointed rock-mass zone was modeled at the surface of the model (Figure 8) to which  $V_s=700$  m/s was assigned based on DH5 (Figure 7c). A  $V_s=1300$  m/s was assumed for the seismic bedrock **at a depth of about 250 m from the ridge surface (i.e., about 500 m a.s.l.)** considering a stiffness increment due to confining stress at depth and measurements carried out in similar geological conditions (Table 2 and Figure 8). We also consider no distinction between arenaceous and pelitic group by assuming that  $V_s$  values become similar at high depth. For landslide cover and alluvial soils,  $V_s$  values equal to 400 m/s and 500 m/s were assumed respectively, **based** on DH and MASW available tests (see upper part of DH\_Ecoscuola in Figure 7c). Regarding the nonlinear properties, the average curves proposed by Rollins et al. (1998) for gravelly soils were employed for landslide cover and alluvial soils given the prevalent coarse grain-size composition. Rocky lithotypes, characterized by high values of stiffness, were considered as linear visco-elastic materials; the damping ratio  $D$  was in the range 0.5% -1%.

Lithotype	$\gamma$ (kN/m <sup>3</sup> )	$V_s$ (m/s)	$\nu$ (-)	Nonlinear material curves
a1a/a3a	19	400	0.45	Rollins et al. (1998)
b/bn1	20	500	0.43	
Jointed rock-mass	22	700	0.38	Linear $D=1\%$
LAG4c-d	23	1000	0.4	Linear $D=0.5\%$
LAG4b	22	900	0.4	Linear $D=1\%$
Seismic Bedrock	24	1300	0.4	-

Table 3. Arquata del Tronto site: **selected parameters for subsoil model used for site response analyses.**

### 3.3 Numerical modelling: results and discussion

The results are reported in the upper part of Figure 8 in terms of amplification factors of spectral acceleration (AF) at surface computed in the period ranges 0.1-0.5s, 0.4-0.8s and 0.7-1.1s. Major amplification effects take place in the 0.4-0.8s period range where amplification of about 2 **characterizes** all the ridge, from the castle (P1 in Figure 8, red box) to the village (P2, blue box). In 0.1-0.5s range a peak  $AF=2$  is attained at P1 while moderate amplification is computed at village ( $AF=1-1.3$ ). Finally, minor amplification effects ( $AF<1.2$ ) can be observed at longer periods (0.7-1.1s). This is substantially compatible with H/V observations: the H/V curves show linear resonance frequencies at ridge in the order of 1-4 Hz (i.e. 0.3-1 s) while the spectral **ratios** are almost flat for frequencies lower than 1 Hz (i.e., period > 1s). It should be noted that, because of the **high material** stiffness and consequent linear model assumed for the ridge, results from numerical analyses and data from H/V can be directly compared.

Average response spectra computed from 2D analyses are compared with average input motion spectrum at P1 and P2 in Figure 8. The comparison substantially confirms that amplification takes place essentially for periods lower than 0.7-0.8s. Spectral accelerations as high as 1.4-1.6g appear at P1 in the 0.2-0.3s period range; on the contrary, the spectral acceleration is lower than 0.8g at P2 in the whole period range.

In order to explore the 2D physical phenomena governing the local response, additional 1D analyses were carried out at P1 and P2 using the same stratigraphic conditions of 2D simulations. Response spectra averaged over the seven accelerograms are therefore compared with 2D and input spectra in Figure 8. Moreover, in the bottom part of the same figure, the 2D/input, 1D/input and 2D/1D spectral ratios are reported. Clear bi-dimensional effects are noticed in P1 at 0.2s and 0.5 s (peaks of 2D/1D ratio); these effects are responsible **for** ground motion amplification in the 0.1-0.5s and 0.4-0.8s period ranges above mentioned; here the 2D analyses double the amplitude of ground motion predicted by 1D simulations. At P2, 1D and 2D results are much closer; however, an evident 2D/1D peak of about 2 **appears** at 0.5s, substantially matching the H/V peak (about 2-2.5 Hz, Figure 7). The use of H/V shows therefore encouraging results in capturing also complex 2D effects as shown by other literature studies (Pagliaroli et al., 2015).

Finally, it should be noted that the amount of amplification predicted by the numerical model satisfactorily **matches** the amplification estimated by the Generalized Inversion Technique (GIT) applied to several recordings carried out with a temporary network installed by the OGS institute after the August 24, 2016 event (Priolo et al. 2019, this issue). In particular, assuming Uscerno as reference rock site, the amplification function at OGS MZ80 station (located close to P1) shows peaks as high as 2-3 in the 1.5-4 Hz range, in which numerical 2D/input peaks of similar amplitude are located (0.2-0.6 s in Figure 8b).

The satisfactory agreement between numerical and experimental amplification functions confirms the substantial reliability of the numerical model.

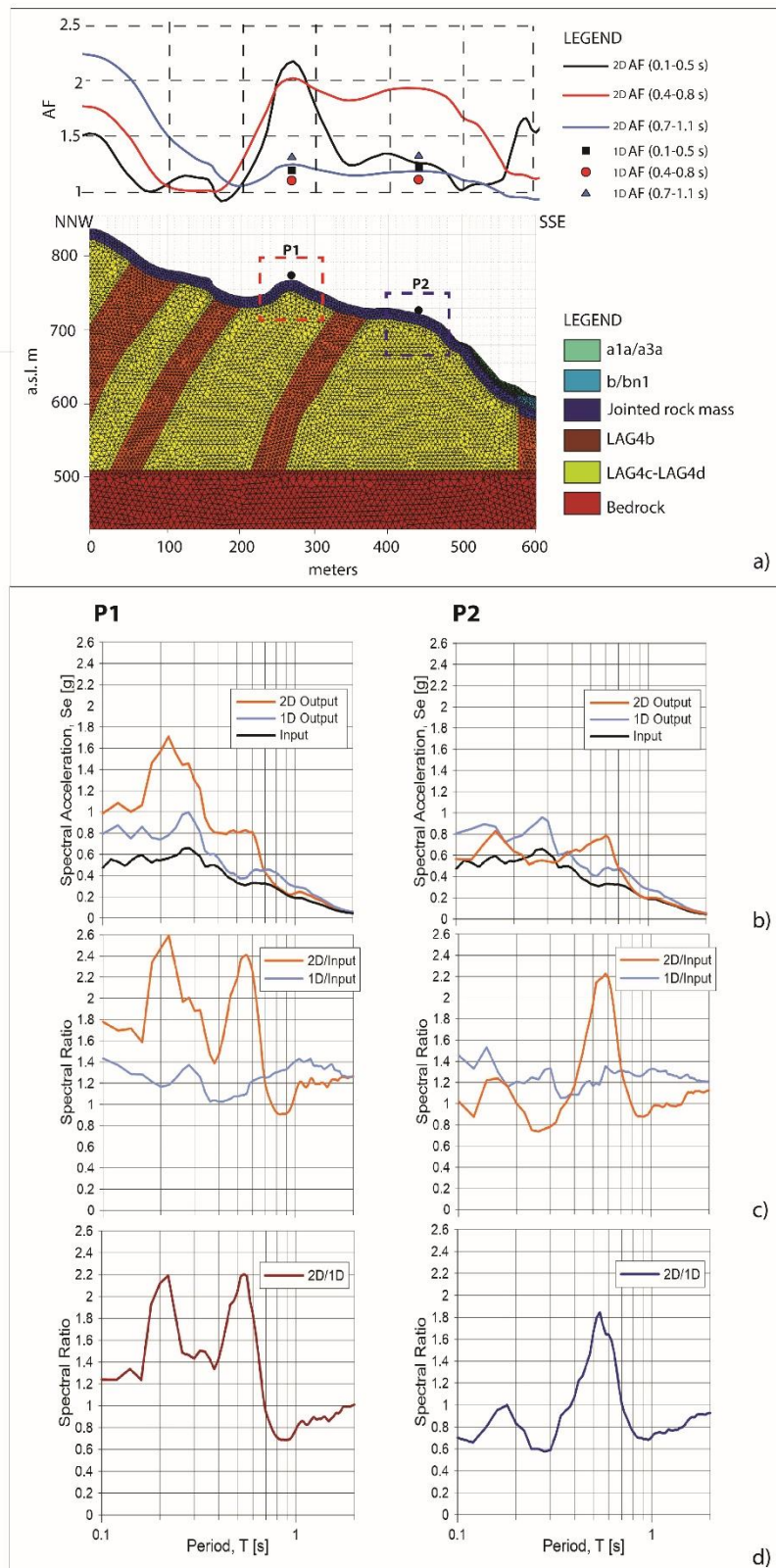


Figure 8. *Arquata del Tronto site*: a) Finite element mesh adopted for Section 1; the labels identify the lithological units described within the text, whose physical and mechanical properties are presented in Table 3. On top of the mesh results of the numerical site response analyses are presented in terms of Amplification Factors (AF) computed in the three period ranges  $T = 0.1-0.5s$ ;  $0.4-0.8s$ ;  $0.7-1.1s$ ; b) average response spectra ( $\zeta=5\%$ ) at P1 and P2 computed through 2D and 1D numerical analyses; c) average 2D/input and 1D/input spectral ratios; d) average 2D/1D spectral ratios at P1 and P2.

## 4.0 Montedinove site

### 4.1 Morphological and geological outlines

Montedinove is a small municipality in the southern part of the Marche region, in the Province of Ascoli Piceno, which extends for 11.9 km<sup>2</sup>. Three different zones of the entire area have been identified for the seismic microzonation: the localities of Lapedosa and Croce Rossa, severely damaged by the 2016 Central Italy Earthquake Sequence, and the most densely populated historical centre.

From the morphostructural point of view the area is characterized by a NE-SW hilly ridge, whose top reaches 561 m a.s.l. Figure 9 shows the lithotechnical map and two relevant cross-sections, which have been selected for the numerical modelling. The geological bedrock is constituted by the Blue Clays Formation (**Formazione delle Argille azzurre: FAA, Regione Marche, 2001**) which is characterized by different lithofacies: conglomeratic, arenaceous, arenaceous-pelitic and pelitic. These lithotypes, following the standard for microzonation, are accordingly identified as ALS (alternation of stratified lithotypes), GRS (granular cemented **bedrock**) and COS (cohesive, overconsolidated stratified **bedrock**). At the ridge crest the geological **bedrock** is outcropping, while on the sides eluvial and colluvial coverings are present with a thickness of 3-15 m. With regards to their compositions, soil cover deposits have been classified as GM (gravels and sandy gravels), SM (sands and silty sands) and ML (low plasticity clayey silts).

The historical centre lies mainly on GRS, locally covered by its **weathered** upper part (SF\_GRS), and on ALS (Figure 9). The deepest portion of the geological sequence is constituted by the upper (COS\_a), the intermediate (COS\_b) and the lower (COS\_c) part of the cohesive, overconsolidated stratified **bedrock**. Additional information about morphological and geological outlines can be found in Amanti et al. (2018, present issue) and Angelici (2018).

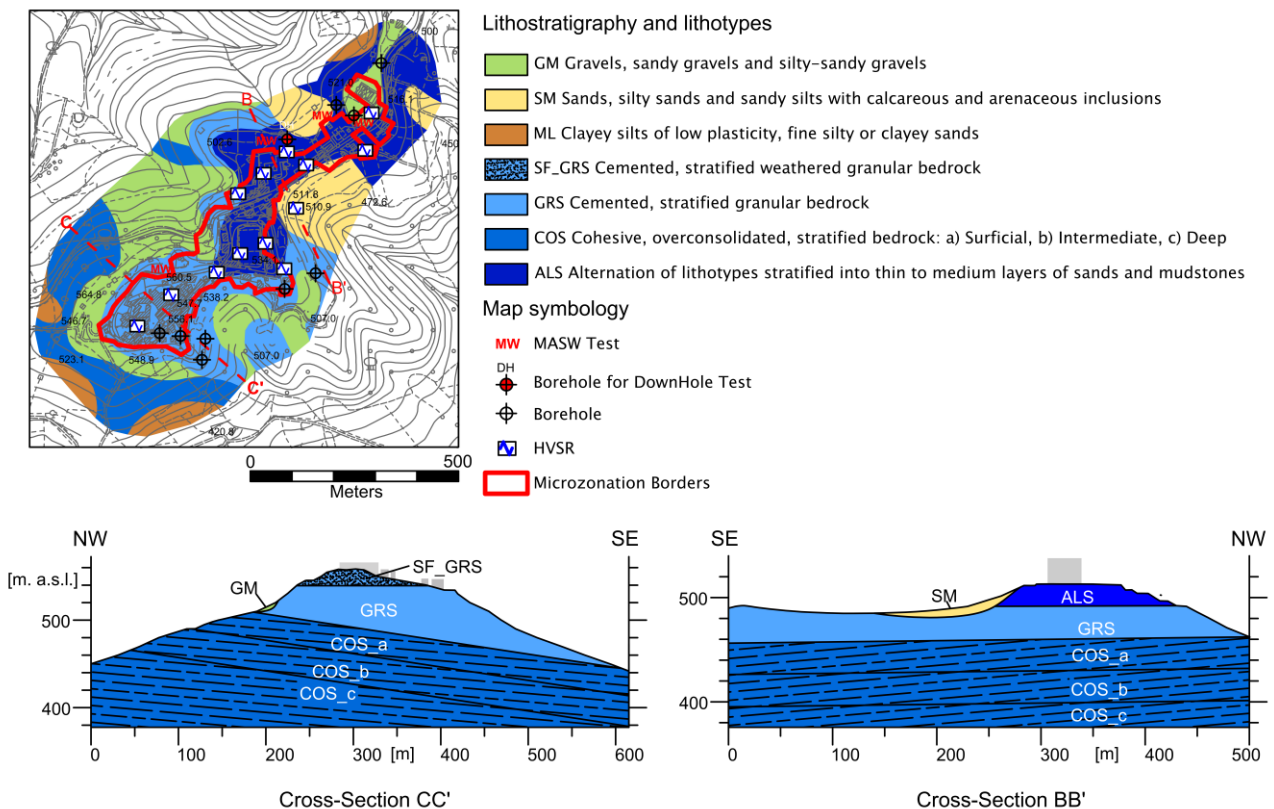


Figure 9. Lithotechnical map and cross-sections of the Montedinove historical centre

### 4.2 Subsoil model

The subsoil model for site response analyses was defined based on in situ geophysical and laboratory tests. Available data from the Level 1 Seismic Microzonation consist of **three** MASW, **one** P-wave SR and **five** HVSR tests. Additional tests were then performed in the framework of the present study to characterize all the geotechnical lithotypes.

Specifically, the new survey included (Angelici, 2018): a 35 m deep DH test, 5 MASW tests and 24 HVSR tests. The location of the full set of investigations is reported in Figure 9.

Figure 10a shows the representative P-wave velocity ( $V_P$ ) and S-wave velocity ( $V_S$ ) profiles from the DH test which involved the ALS, the GRS and the SM lithotypes. The other materials were characterized by non-invasive tests. The geotechnical model for site response analyses is summarized in Table 4.

The nonlinear cyclic response of the COS was investigated by means of a RC test performed on a sample from the nearby municipality of Monte Rinaldo (Ciancimino et al. 2019, this issue). Given the lack of specific laboratory tests, predictive models proposed in literature for similar materials were adopted for the other lithotypes. Details are reported in Table 4, while Figure 10b shows the normalized shear modulus and damping ratio curves.

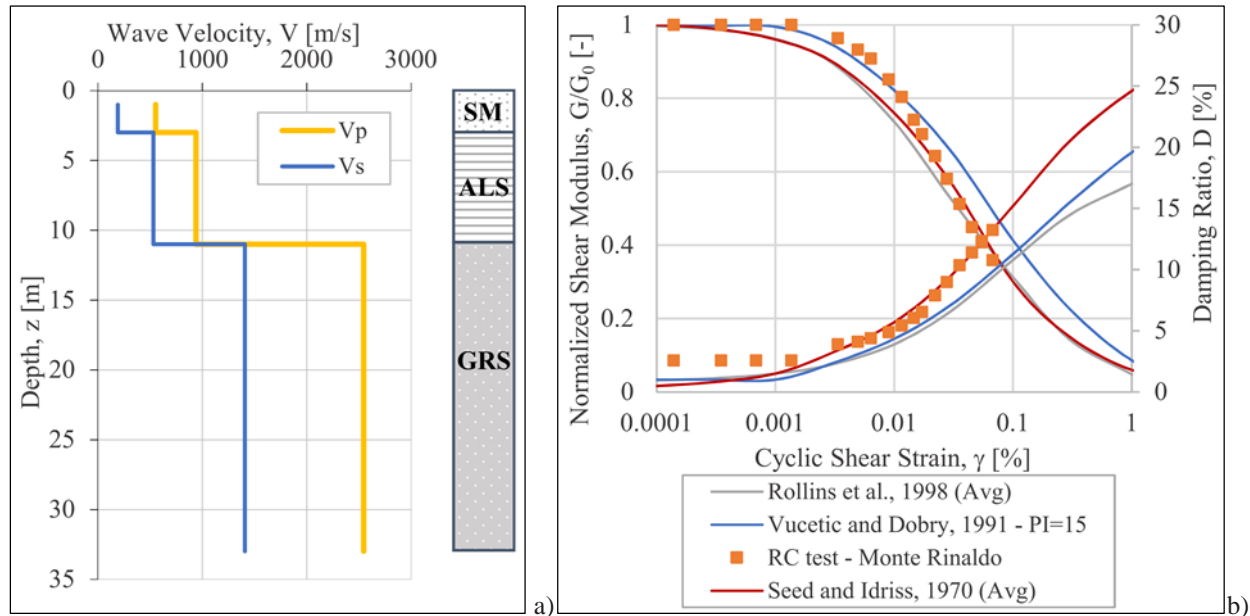


Figure 10. Subsoil model for Montedinove site: a) P-wave velocity ( $V_P$ ) and S-wave velocity ( $V_S$ ) profiles from the DH test; b) normalized shear modulus and damping ratio curves.

Lithotype	$\gamma$ (kN/m <sup>3</sup> )	$V_s$ (m/s)	$\nu$ (-)	Nonlinear material curves
SF_GRS	19.0	550	0.35	Rollins et al. (1998)
GRS	22.0	1400	0.28	Linear Viscoelastic - $D_0 = 0,5\%$
GM	18.6	340	0.35	Rollins et al. (1998)
SM	17.6	190	0.43	Seed and Idriss (1970)
ALS	19.6	530	0.27	Vucetic and Dobry (1991) PI=15
COS_a	19.6	560	0.46	RC Test (Monte Rinaldo)
COS_b	19.6	650	0.46	RC Test (Monte Rinaldo)
COS_c	19.6	800	0.46	Linear Viscoelastic - $D_0 = 0,5\%$

Table 4. Montedinove site: selected parameters for subsoil model used for site response analyses.

The main challenge in the definition of the subsoil model was the identification of the seismic bedrock. The HVSR tests carried out on the ridge crest highlighted high fundamental frequencies (10-15 Hz) consistent with the impedance contrast between the SF\_GRS or the ALS and the underlying GRS. Considering the high  $V_S$  value (1400 m/s) obtained by the DH test for GRS (Figure 10a), this might lead to identify the GRS as the seismic bedrock. However, in the whole region the GRS is underlain by COS lithotype which is characterized by medium  $V_S$  (550-650 m/s) leading to a significant shear wave velocity inversion in the subsoil. The  $V_S$  of COS increase with depth, slowly reaching values characteristic of the seismic bedrock (~800 m/s). This geological evidence was subsequently confirmed by the MASW and HVSR tests performed in the near Lapedosa locality, which allowed to define the deepest part of the stratigraphic sequence. The COS unit was then subdivided into three subunits (COS\_a, COS\_b and COS\_c) with an increasing  $V_S$  profile and COS\_c assumed as seismic bedrock.



### 4.3 Numerical analyses: results and discussion

In order to check the influence of seismic bedrock assumption on site response, two hypotheses were analysed: bedrock at the top of the GRS formation (Shallow Bedrock, SB), i.e. without modelling the underlying COS, and bedrock constituted by the COS\_c (Deep Bedrock, DB). Results are reported for the two cross-sections in the spectral contour plots (Figure 11a) in terms of ratio between the elastic average response spectra amplification factors defined in the three period ranges  $T = 0.1-0.5\text{s}$ ;  $0.4-0.8\text{s}$ ;  $0.7-1.1\text{s}$ .

Firstly, site response at the ridge crest is commented (see cross-section C-C' in Figure 11). At low periods ( $< 0.5\text{ s}$ ), as expected, the damping of the high frequencies due to the propagation in COS\_a and COS\_b is noticed thus resulting in low  $S_{e,DB}/S_{e,SB}$  ( $\sim 0.4-0.7$ ). On the other hand, the lower fundamental frequencies of the DB models lead to a higher amplification at intermediate and high periods where  $S_{e,DB}/S_{e,SB}$  is higher ( $\sim 1.1-1.3$ ). A different response is observed at the NW flank of cross-section CC': the outcropping units of the COS (COS\_a, COS\_b) lead indeed to a low periods amplification given by the impedance contrast with the deeper part (COS\_c). This effect obviously is not considered in the SB model. Consequently, high  $S_{e,DB}/S_{e,SB}$  values ( $\sim 2$ ) are observed for  $T=0.2-0.4\text{ s}$ .

On the basis of the available information, the hypothesis of DB was considered the most suitable and the amplification factors obtained from the DB models were therefore used for the Level 3 of the Montedinove seismic microzonation.

Finally, to highlight the role of 2D effects, Figure 11c reports the results of the 2D DB analyses and the corresponding 1D equivalent-linear analyses in terms of elastic response spectra and 2D/1D spectral ratios at the ridge crest. The results confirm the frequency-dependence of the **topographic effects and that the amount of amplification** increases for steeper topographies as highlighted by previous studies (e.g., Pagliaroli et al., 2011): topographic effects are higher for steeper section CC' with respect to the gentle slope section BB'. Both sections show the relevance of topographic effects for periods lower than 1 s. For the section BB' topographic effects are on average consistent with the simplified approach proposed by the technical codes (Eurocode 8 or Italian NTC2018). Topographic amplification factors (up to 3), higher compared to the simplified factors, are instead detected for the steeper section CC'. In particular, for section CC' the maximum topographic effect takes place at 0.2-0.3s; this period corresponds to the 2D resonance of the upper part of the ridge (above 5000 m a.s.l.) constituted by GRS as estimated by simplified formula proposed by Paolucci (2002).

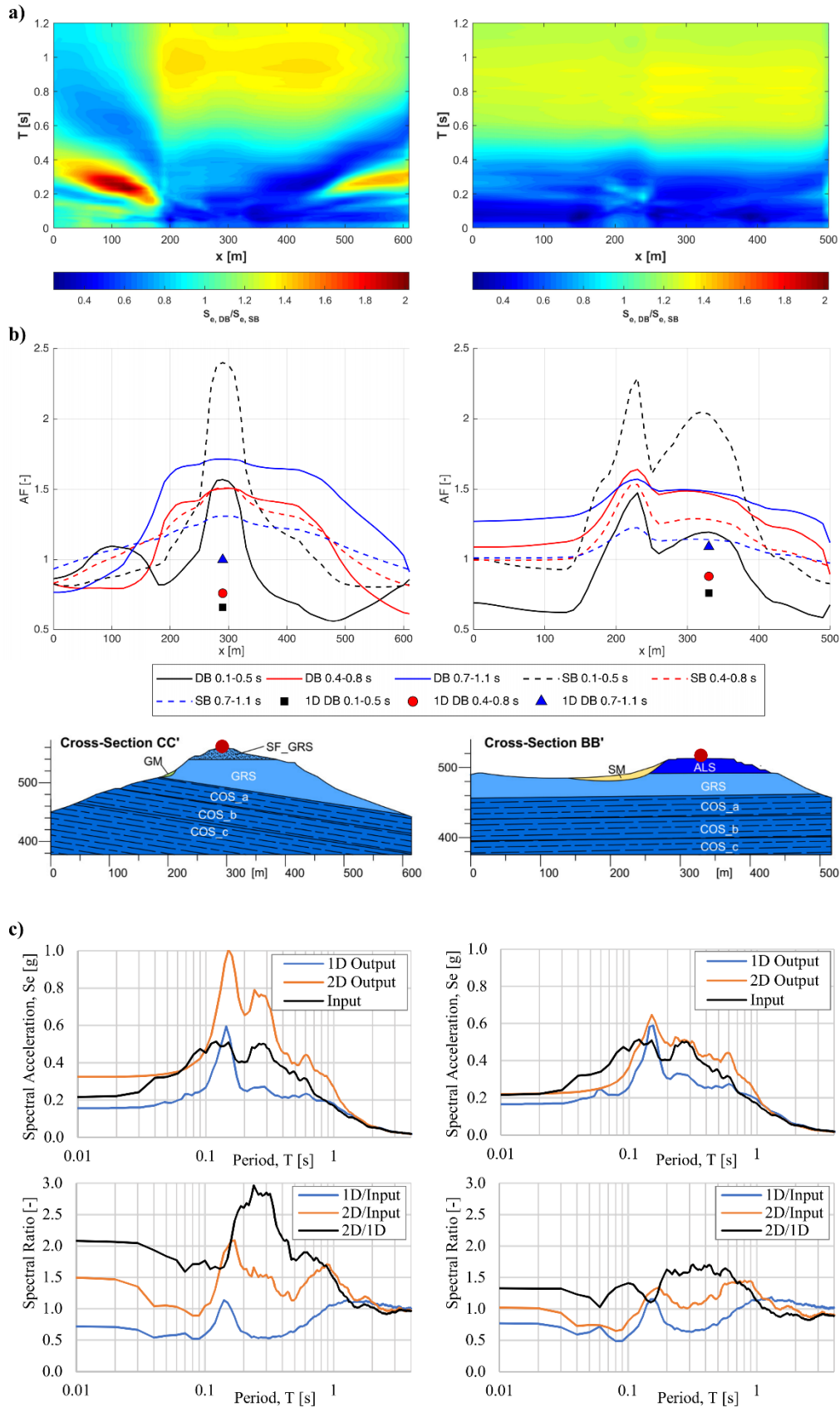


Figure 11. *Montedinove site*: results of the site response analyses for cross sections CC' (left) and BB' (right): a) contour plots of the ratio between the elastic average response spectra ( $\xi=5\%$ ) from the DB and the SB models; b) Amplification Factors computed in the three period ranges  $T = 0.1-0.5s$ ;  $0.4-0.8s$ ;  $0.7-1.1s$ ; c) response spectra ( $\xi=5\%$ ) and spectral ratios from the 2D and 1D DB numerical analyses computed at the ridge crest (red points in the cross-sections).

## 5.0 Capitignano site

### 5.1 Morphological and geological outlines

The Capitignano village is located in Abruzzo region, about 20 km north of the city of L'Aquila. It is placed in the north-eastern sector of the Montereale Basin (MB), a Plio-Quaternary intermontane basin located southeast to the Amatrice Basin, along the axial zone of the Apennine chain (Cosentino et al., 2017).

The MB, extending over an area of about 20 km<sup>2</sup>, has a triangular shape with a straight north-eastern margin related to the presence of the NW-SE trending Capitignano Fault, whose extensional activity is responsible for the onset and evolution of the MB during Plio-Quaternary. The Capitignano Fault belongs to the normal active fault system to which is related the Mw = 6 earthquake of the January 16, 1703 (Boncio et al., 2004; Civico et al., 2016).

The Capitignano Fault is composed by several segments characterized by a normal slip kinematic, with a minor left lateral component, along W dipping NW-SE trending planes mainly occurring in the syn-orogenic terrigenous deposits (Laga Fm., upper Miocene), with a stratigraphic offset ranging from 400 to 600 m (Chiarini et al., 2014).

The MB morphology is related to the Plio-Quaternary activity of the Capitignano Fault that brings to the formation of a wide piedmont belt formed by coalescent Pleistocene alluvial fans developed in the NE sector, in correspondence of the fault boundary (Figure 12). This piedmont belt degrades with a gentle slope toward SW and is connected, through a series of Holocene alluvial fans entrenched into the older ones, to the alluvial plain of the Mozzano Creek which extends to the W up to the confluence with the Aterno River (GM, SM and ML in Figure 12).

At the NE margin of the MB, the footwall of the Capitignano Fault, is characterized by a N240° dipping monocline formed by fractured or weathered sandstones of the Laga Fm. (Campotosto member: LAG4) (SFLPS in Figure 12). The Plio-Quaternary basin infill is mainly represented by subsequent generation of alluvial fans, passing toward W to fluvial and lacustrine sediments interfingering with debris flow and colluvial deposits at the basin boundary (GM, SM and ML in Figure 12). Chiarini et al. (2014) recognize four different geological units within the MB referable to the Early Pleistocene-Holocene. The continental deposits show thickness generally higher than 100 m below the alluvial plain (P10, P49, P119: Figure 12), with a maximum thickness of about 200 m in the hanging-wall of the Capitignano Fault, as highlighted by geophysical data (Chiarini et al., 2014; Tallini et al., 2017). Furthermore, boreholes data show a thickness decrease of the Quaternary deposits from 40-50 m (P107) to 15-20 m (P8) to 0 m moving from the westward to the eastward splay of the Capitignano Fault (Figure 12b).

Section BB' (Figure 12b), well constrained by many boreholes and geophysical investigations, is representative of the geological array of the Capitignano area, common to many others intermontane basin of the Central Apennine. It shows the tectonic boundary between the piedmont belt of the MB and the 70° SW dipping Capitignano Fault system formed, here, by four tectonic elements with an estimated fault zone of about 400 m. The footwall of the Capitignano Fault is characterised by the outcropping of Laga Fm. formed by a 10 m-thick horizon of weathered sandstone (i.e. the regolith layer) (SFLPS) laid on fresh sandstone (LPS). Conversely, the hangingwall is composed by about 140 m-thick of alluvial-lacustrine and detrital Quaternary deposits.

The presence of the Capitignano Fault represents a significant lateral seismic impedance contrast which suggests probable 2D seismic amplification effect, that were analysed through 2D numerical modelling of section BB'.

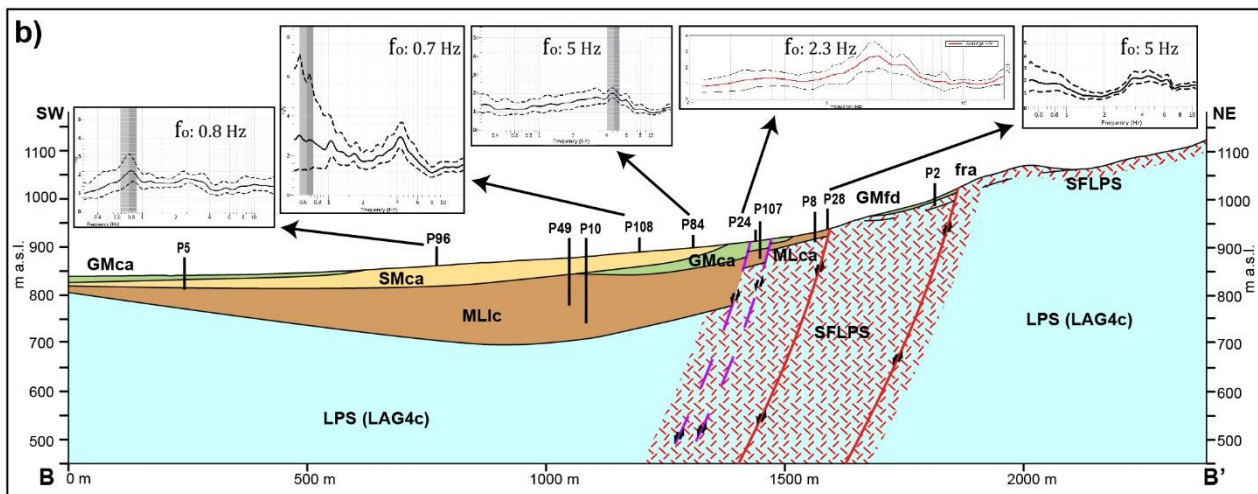
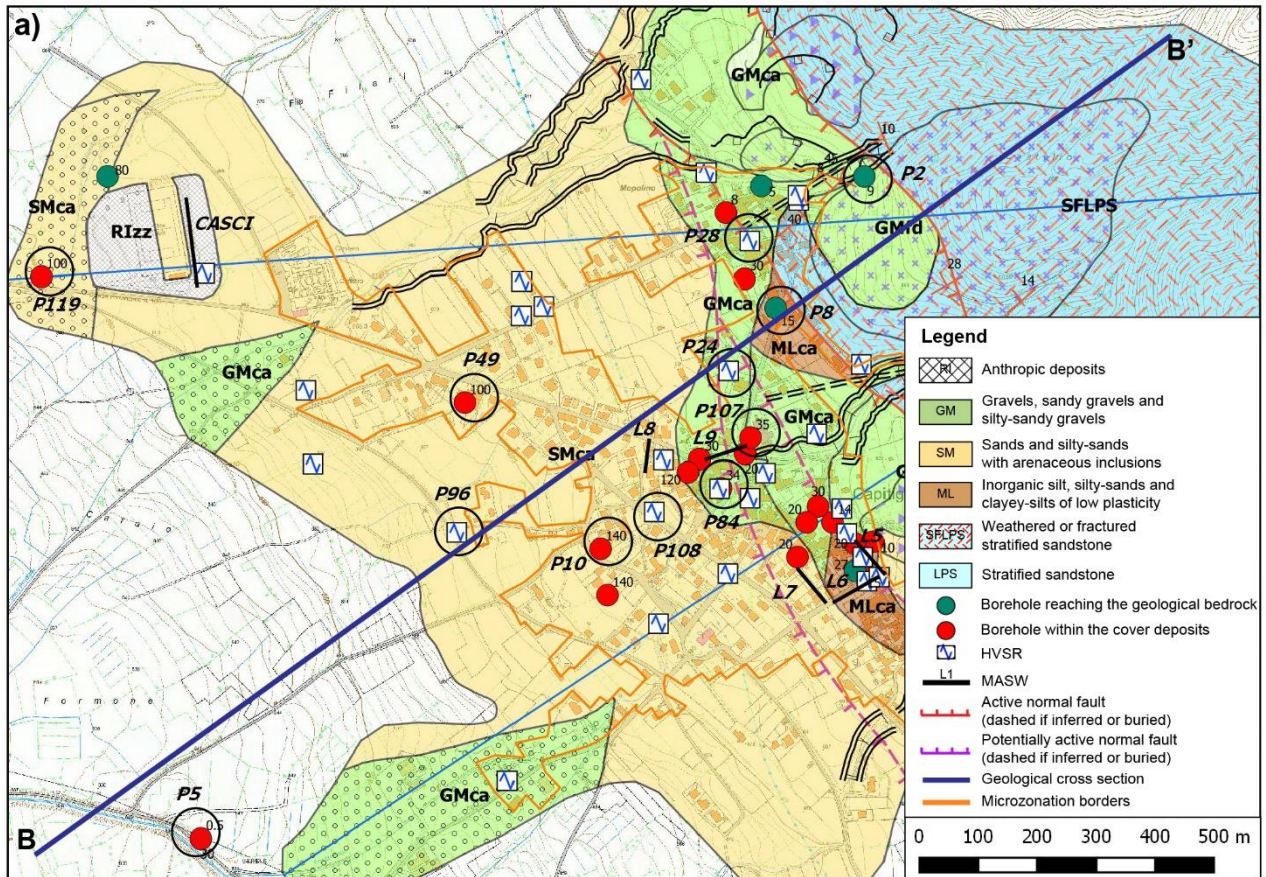


Figure 12. a) Lithotechnical map of the Capitignano area; b) Cross section BB' used for the numerical modelling. LPS = seismic bedrock (Laga Fm.); SFLPS = weathered or fractured geological bedrock (Laga Fm.); GMca, GMfd (green) = gravel and sandy gravel with silt, of alluvial fan and talus cone origin respectively; SMca (yellow) = sand and silty sand of alluvial fan origin; MLic, MLca (light brown) = inorganic silt and clayey silt of lacustrine and distal alluvial fan origin; RIzz = anthropic deposits. Borehole used to elaborate the BB' cross-section: red spot, borehole quoted in the text: black circle.

## 5.2 Subsoil Model

The subsoil model of section BB' used for the numerical simulation has been defined by considering several geophysical and geotechnical investigations, among which about 30 boreholes, HVSR measurements, down-hole and MASW (Figure 12a). Representative results from MASW (L5-9) and DH (P107) investigations are reported in Figure 13.

The seismic bedrock depth was estimated through the combined use of geophysical investigations, noise and earthquake measurements (CNR-IGAG, 2017; Tallini et al., 2017) and the 100 m-deep borehole (P119) (Chiarini et al., 2014). In the deepest sector of the basin,  $f_0$  from noise and weak motion is about 0.8 Hz, caused by the overlap of the thick Quaternary sequence onto the Laga Formation. At Capitignano village, close to the valley edge,  $f_0$  is about 3.5-4.5 Hz due to the presence, within the multi-layered Quaternary sequence, of a gravel layer (GM) below the sandy deposits (SM). Close to the footwall of the Capitignano Fault, HVSR recordings show broad peak in the range of 3-6 Hz, which is probably due to the thin layer of Pleistocene silt (ML) on the regolith layer of the Laga Fm. (SFLPS) (Figure 12). The adopted physical and mechanical parameters and the nonlinear curves are reported in Table 5 while a sketch of the numerical model is represented in Figure 14b.

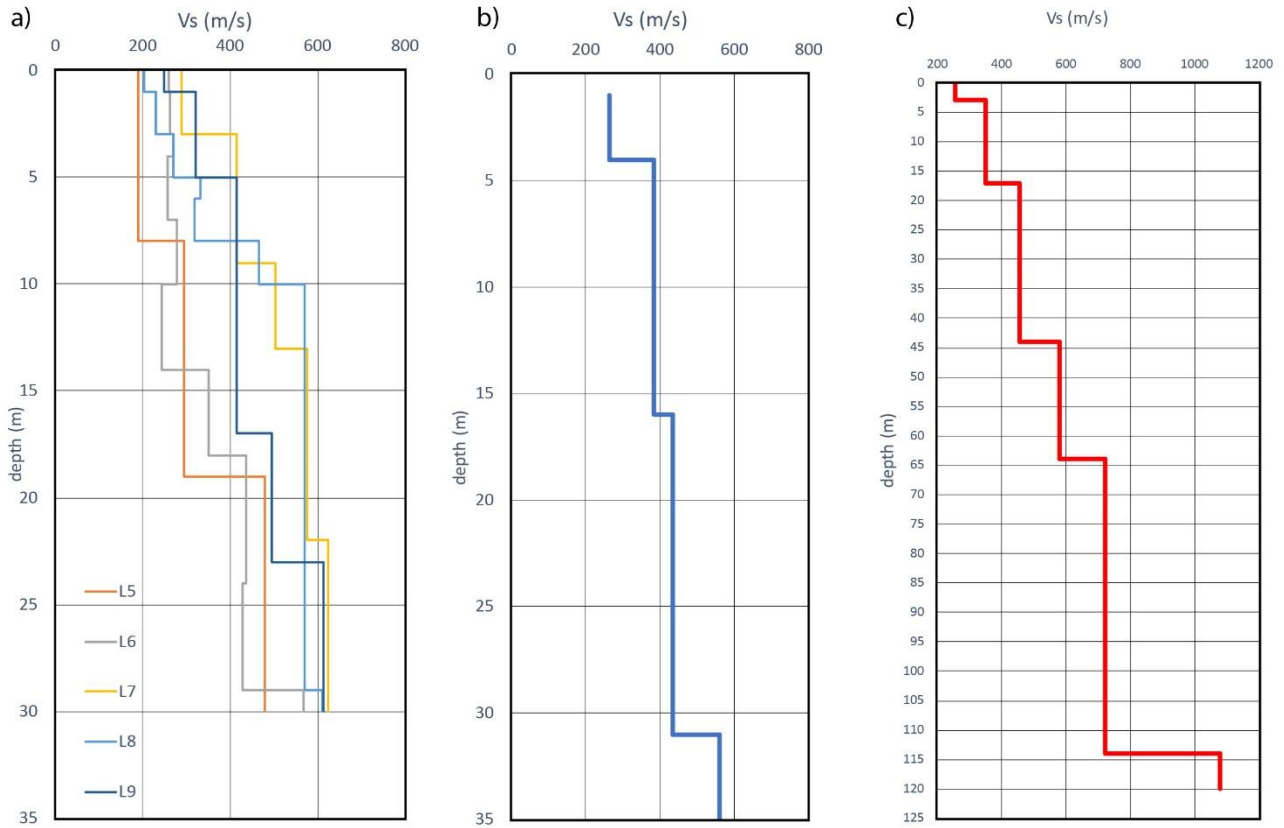


Figure 13. Representative  $V_s$  profile obtained from MASW (a), down-hole (b) and joint inversion technique of active (MASW) and passive (ESAC, HVNSR) investigations at Casci site (c) (modified from Tallini et al., 2017); for their location see Figure 12.

Lithotype	$\gamma$ (kN/m <sup>3</sup> )	$V_s$ (m/s)	$\nu$ (-)	Nonlinear material curves
Silty sand SM	18.5	300	0.40	Seed and Idriss (1970) mean
Gravel GM	19	300-450	0.40	Rollins et al. (1998) average
Silt, silty sand, clayey silt ML	18.5-19	600-750-900	0.35	Darendeli (2001) PI=30
Geological bedrock Highly fractured sandstone SFLPS	19.5	750, 900	0.38	Linear D=1%
Geological and seismic bedrock Sandstone LPS	23	1300	0.25	Linear D=0.5%

Table 5. Capitignano site: *selected parameters for subsoil model used for site response analyses.*

### 5.3 Numerical modelling: results and discussion

The amplification factors computed through 2D analyses along the BB' section surface are reported in Figure 14c. The amplification factors of the thick multi-layered infill of MB, in the Capitignano Fault hangingwall, reach a maximum value of about 1.4, 2.6 and 3.4 for the three period ranges (0.1-0.5s, 0.4-0.8s and 0.7-1.1s); several peaks are attained in the amplification factors profiles along the basin infill showing significant ground motion variations for distance of the order of 100-200 m. This pattern is due to 2D effects probably related to the propagation of lateral surface waves generated at the edge (i.e., fault zone) interacting with direct waves. This is typical of shallow and large basin. The contours of peak ground acceleration (Figure 14d) well match the medium-to-high frequency  $AF_{0.1-0.5s}$  profile, showing maximum values as high as 0.4g. The amplification factors in the footwall **decrease** sharply reaching unity for all the considered period ranges (Figure 14c) while a moderate amplification (factors comprised between 1 and 2) is noticed in correspondence of the highly fractured sandstone SFLPS.

In order to quantify the 2D effects, the mean acceleration response spectra obtained with the 1D and 2D modelling have been calculated for three specific sites (Figure 15a):

Site A: plain morphology of the MB filled by the multi-layered detrital units (SM, ML) ( $V_s$ : from 450 to 900 m/s);

Site B: weathered sandstone (SFLPS) ( $V_s$ : 750 m/s) onto the Capitignano Fault damage zone (SFLPS) ( $V_s$ : 900 m/s);

Site C: weathered sandstone (SFLPS) ( $V_s$ : 750 m/s) onto the fresh sandstone (LPS) ( $V_s$ : 1300 m/s).

For site A, the comparison between 1D and 2D modelling shows 2D PSA weakly higher than 1D PSA for low periods, while, at medium-high periods, 2D PSA is heavily higher than 1D PSA evidencing remarkable bidimensional effects due to buried morphology (Figure 15b). An aggravation factor AGF (Riga et al., 2016) of about 2 with respect to 1D prediction has been computed for periods equal or higher than 1 s.

Overall, the results here obtained match the findings obtained by Riga et al. (2016) based on extensive parametric 2D numerical linear viscoelastic analyses carried out on homogeneous asymmetric large alluvial basins. In particular, in the study by Riga et al. (2016), for a shape ratio of 0.2 and for high slope edge angles (similar to geometric condition pertaining to the Capitignano basin), AGF in the range 1.5-2 are computed at a normalized distance  $x/w = 0.35$  (where  $x$  is the distance from the edge and  $w$  the length of the valley) corresponding to point A. These values are associated to the period range  $1-1.5 T_{0,c}$  where  $T_{0,c}$  is the 1D fundamental period at the center of the basin; for Capitignano  $T_{0,c}$  is equal to about 0.75s leading to a period range 0.75-1.12s. It should be stressed that the conclusions by Riga et al. (2016) are based on viscoelastic linear analyses and then the role of soil nonlinearity was not addressed. Moreover, the Authors considered a homogenous material filling the basin; 2D effects can be higher in heterogeneous media or in the presence of a shear wave velocity gradient (Bard and Gariel, 1986).

Conversely, at sites B and C, we find better agreement between 1D and 2D modelling, indicating minimal bi-dimensional effects compared to site A (Figure 15c, d).

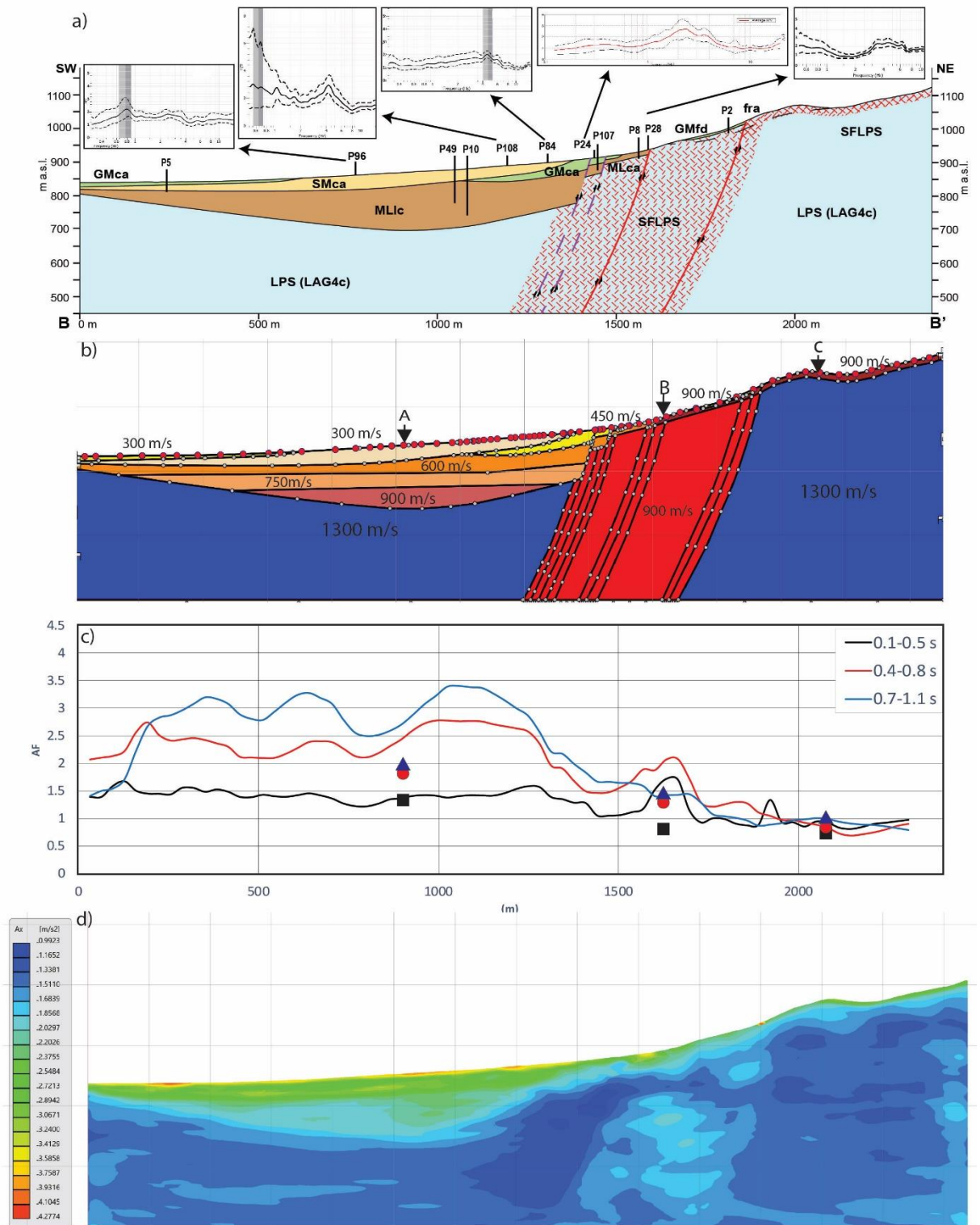


Figure 14. *Capitignano site*: a) Lithotechnical section BB'; b) subsoil model; c) 2D amplification factors for each site placed, every 30 meters, along the section and 1D amplification factor for Sites A-B-C selected on the section d) Contour map of the maximum acceleration (PGA).

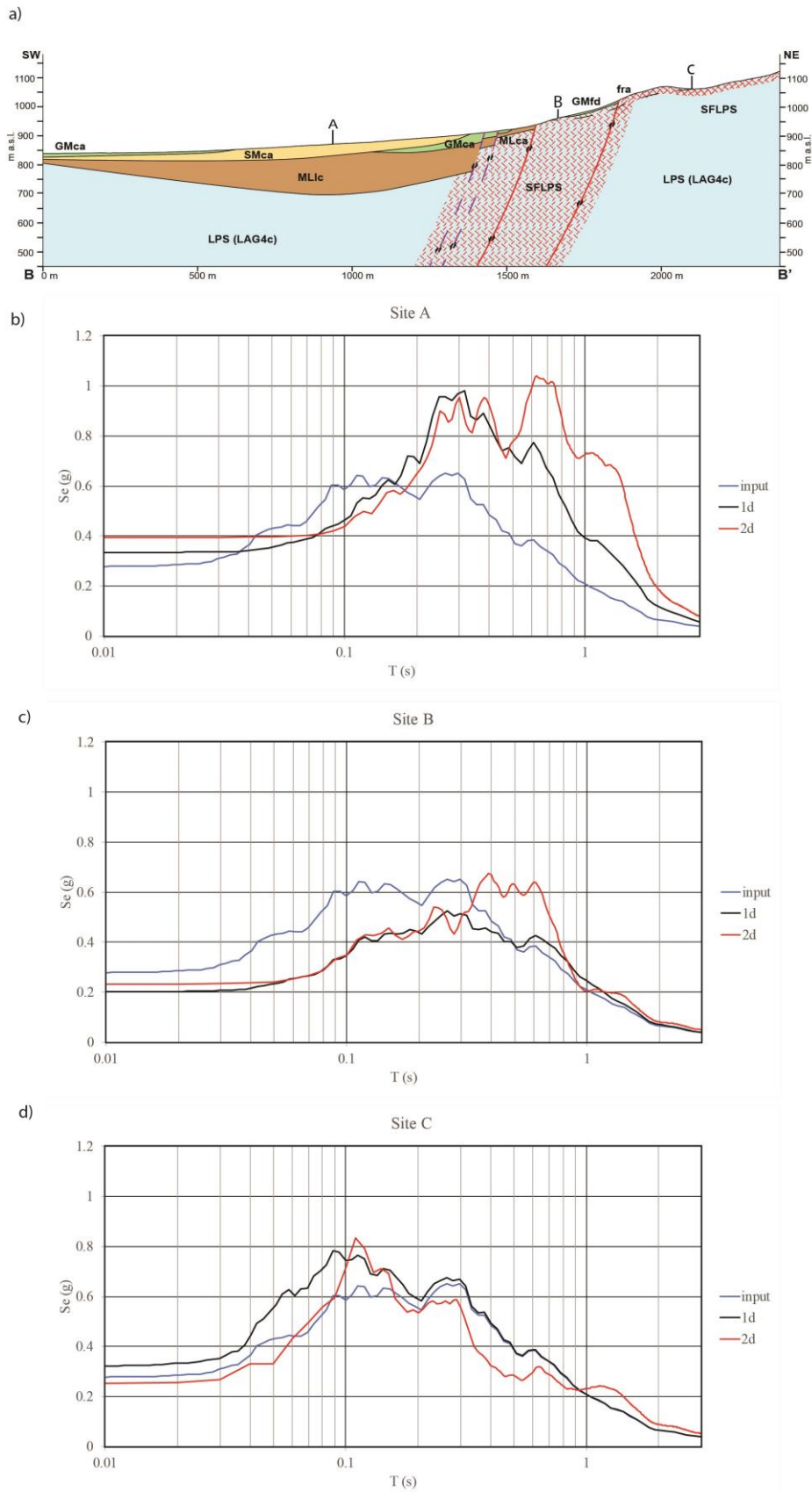


Figure 15. Mean elastic response spectra obtained with 1D and 2D modelling at three specific sites along the BB' section in Capitignano site; a) Site A: Fault hangingwall, MB basin; b) Site B: Fault damage zone; c) Site C: Fault footwall.



## 6.0 Norcia Site

### 6.1 Morphological and geological outlines

The Norcia basin (Figure 16) is a rectangular shaped plain, 10km-long and 3km-wide and represents a typical Plio-Quaternary **intermontane** basin in central Italy (e.g., D'Agostino et al., 2001; Galadini et al., 2003). The **Quaternary** evolution of the **basin** has been driven by two NW-SE striking conjugates normal faults, during the Quaternary (Blumetti, 1995) and the recent activity of the main eastern **boundary** fault has been described by geomorphological and paleoseismological works published since the 90's (e.g. Blumetti, 1995; Galadini and Galli, 2000; Galli et al., 2005). Additional description can be found in Amanti et al. (2019, this issue).

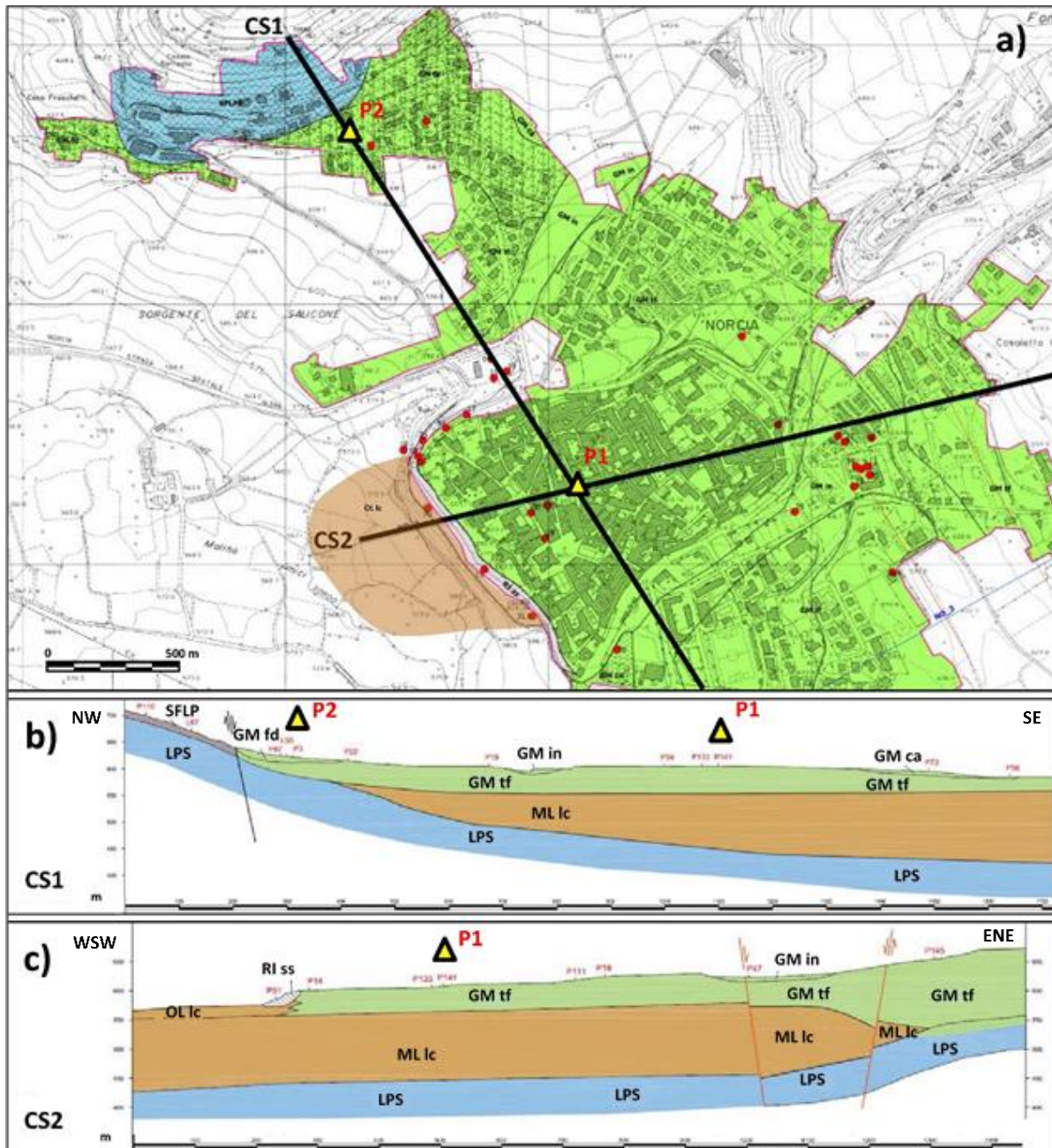


Figure 16. **Norcia site**: a) Litotechnical map, 2D cross-sections (CS1 and CS2) and location of the investigated sites (P1 and P2); b) Cross section CS1; c) Cross section CS2; legend of lithotypes: LPS = seismic bedrock; SFLPS = weathered seismic bedrock; GMfd, GMca, GMin, GMtf = gravel and sand with silt; MLlc = inorganic silt; OLlc = organic silt; RIzz and RIss = anthropogenic deposits.

The basin is filled by **slope** debris, lacustrine and alluvial sediments, whose thickness reaches about 150 m in the centre of the plain. These deposits have been classified in the lithotechnical units GM (gravel and sand with silt), ML (inorganic silt) and OL (organic silt); locally, along the historical city walls, anthropogenic deposits have been found (Figure 16).

Two cross sections (CS1 and CS2, Figure 16) have been drawn, in order to show the vertical and horizontal stratigraphic relationships between the different units; in particular, in correspondence of the historical centre (see cross-sections in Figure 16b), lacustrine deposits (ML) underlie debris deposits (GM). The plio-quadernary deposits are located above the carbonatic units, characterized by limestones and marls, which represent the seismic bedrock.

## 6.2 Subsoil model

The low depth /semi-length ratio (about 0.1) of the Norcia plain indicates a large valley that, in relation to seismic response, can be modelled with a 1D approach. For large valleys, 2D resonance phenomena can be excluded and the seismic response is mainly characterized by one-dimensional resonance and surface wave propagation (Bard and Bouchon 1985). These latter are generally attenuated in the central part of the plain where the response is therefore essentially 1D. As matter of fact, recent studies (Luzi et al. 2019b) have demonstrated that strong-motion recorded in the Norcia plain are dominated by S-waves when earthquakes are characterized by large magnitudes and short distances (from the plain) and the seismic response can be approximated to 1D S-wave propagation. On the contrary, the generation of low frequency (e.g., 0.5 - 1.2 Hz) late arrivals (e.g. surface waves), with amplitudes larger than the S-phase, can be generally associated **with** earthquakes originating at distances greater than 30 km along the Apennine belt. For the Seismic Microzonation study the most conservative hypothesis is formulated, which is the occurrence of earthquakes at short distance, that implies a numerical 1D analysis. However, a comparison between 1D and 2D analyses in Norcia historical centre, at middle valley, is presented in the following to confirm **the** 1D modelling assumption.

Two sites, representing different stratigraphic conditions, have been selected (P1 and P2 in the map of Figure 16). The two selected sites are characterized by different stratigraphic settings: P1, in the historical centre at middle valley, is underlied by GM deposits (45 m) over ML (100 m), with an inversion of the S-wave velocity; P2, at northern edge of the valley, is characterized by GM deposits (30 m) over the seismic bedrock (see the seismically homogeneous microzones map in Figure 17).

The subsoil model has been defined after geophysical and geotechnical investigations. Pre-existing data have been collected (30 boreholes, 31 HVSR, 28 MASW, 28 SR, 2 ERT, 6 REMI and 2 ESAC), and, in addition, new geophysical and geotechnical investigations have been carried out (1 borehole until 35 m depth where an undisturbed soil sample at 30 m was retrieved, 11 HVSR, 5 ESAC, 1 MASW and 1 SR). The location of all investigations is shown in Figure 18 and details on the geophysical investigations can be found in Caielli et al. 2019 (this issue). In Table 6 the subsoil model for the two analysed sites (P1 and P2) is presented.

Unit	P1			P2		
	Thickness (m)	$\gamma$ (kN/m <sup>3</sup> )	Vs (m/s)	Thickness (m)	$\gamma$ (kN/m <sup>3</sup> )	Vs (m/s)
GM	10	19.5	400	15	19.0	250
	15	19.5	600	10	19.5	400
	15	19.5	500	5	19.5	500
ML	70	19.6	400	-	23.0	1100
	50	19.6	550			
Seismic Bedrock	-	23.0	1100			

Table 6. Norcia site: **selected parameters for subsoil model used for site response analyses**

The nonlinear properties of the soil units have been considered through the  $G/G_0$ - $\gamma$  and  $D$ - $\gamma$  curves; in particular, for the GM unit the curves proposed by Rollins et al. (1998) have been selected, whereas for the ML unit specific curves, deriving from laboratory tests on the collected sample, have been adopted. Details on the laboratory tests can be found in Ciancimino et al. 2019 (this issue).

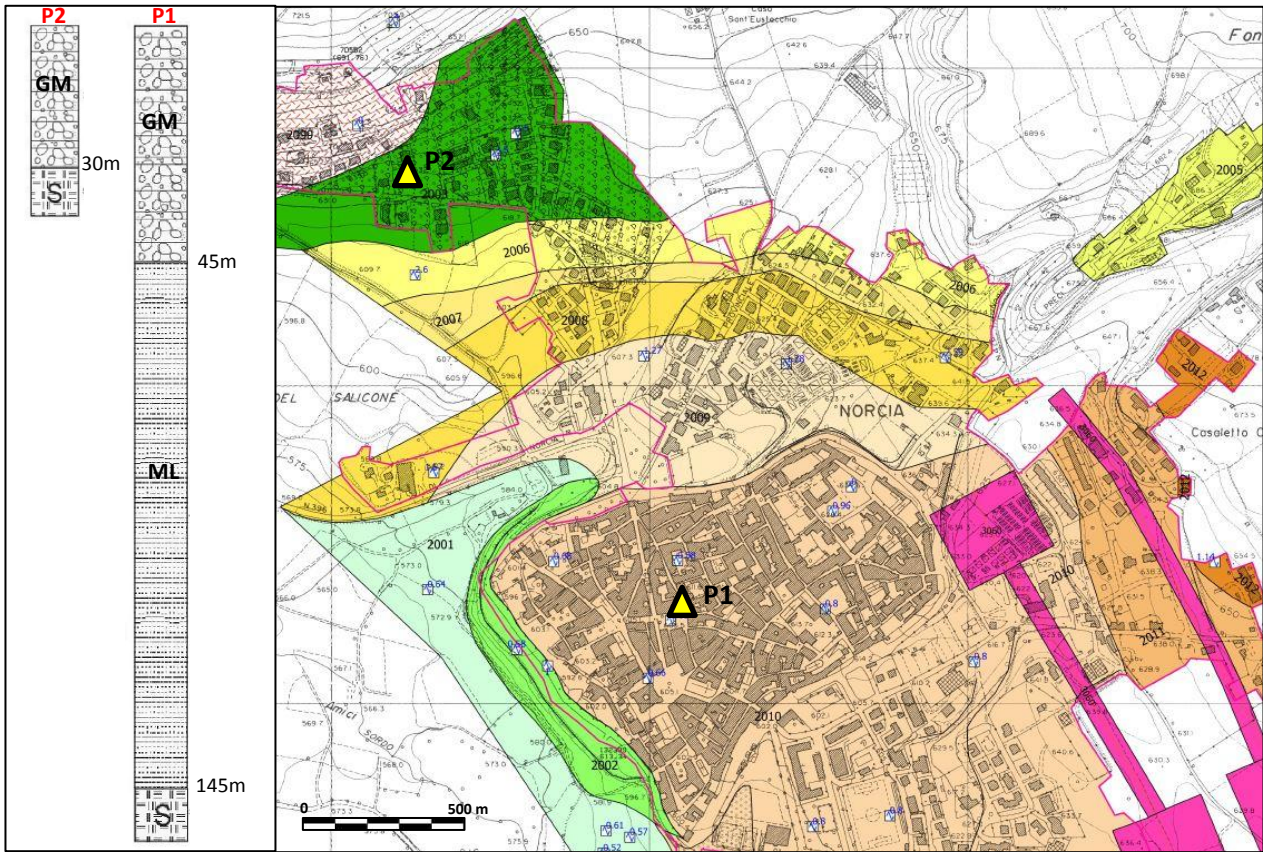


Figure 17. *Norcia site*: map of the seismically homogeneous microzones: colours indicate different lithostratigraphic settings (in purple the active faults buffer zones); sketches on the left illustrate the lithostratigraphy of the investigated sites (GM = gravel and sand with silt; ML = inorganic silt; S = seismic bedrock).

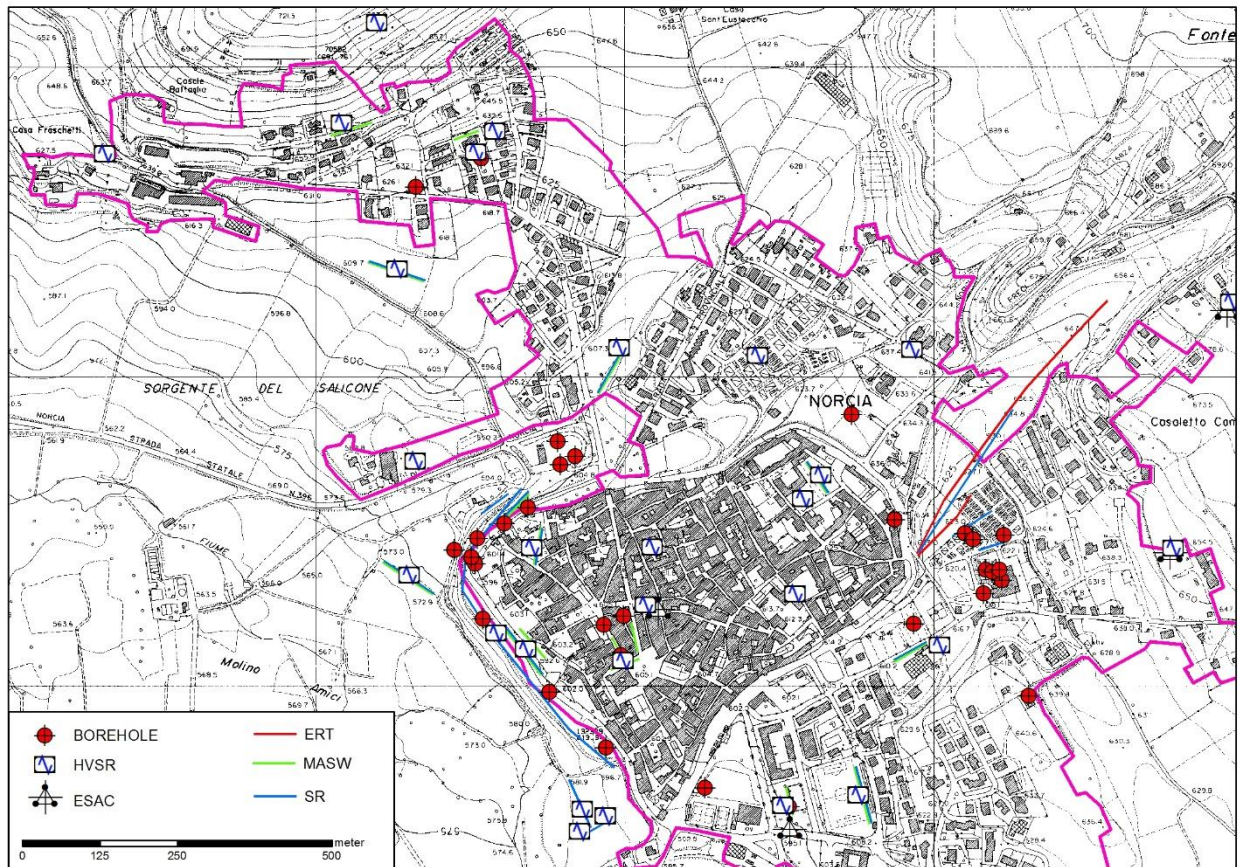


Figure 18. *Norcia site*: map of the geophysical and geotechnical investigations.

### 6.3 Numerical modelling: results and discussion

The numerical analyses have been performed using a 1D S-wave propagation approach. The results are shown in Figure 19 and 20, in terms of amplification factors and acceleration response spectra at the two sites P1 and P2. The different seismic response of the two selected sites is mainly due to the presence/absence of the inversion of the S-wave velocity; in case of presence of the velocity inversion (site P1) the response spectra ordinates are lower **compared to** site P2, because a substantial amount of the energy is trapped and dissipated within the soft layer due to nonlinear behaviour.

In Figure 20 the mean of the input spectra and the mean of the output spectra at sites P1 and P2 are shown, together with the acceleration response spectra of the Italian seismic code (NTC18) for sites P1 (subsoil category B) and P2 (subsoil category C). The results of this study are **consistent** with the NTC18 response spectra for site P1, while, on the contrary, in case of site P2, the NTC18 spectra are not sufficiently conservative, especially for the period range 0.4-0.7 s.

In order to quantify the 1D behaviour at the **center** of the valley an equivalent linear 2D analysis has been performed along the CS1 section. The results at P1, in term of acceleration response spectra are shown in Figure 21, **indicating** that the ground motion amplification is therefore mainly due to stratigraphic effects which are well-predicted by 1D seismic response analysis while 2D effects are almost negligible.

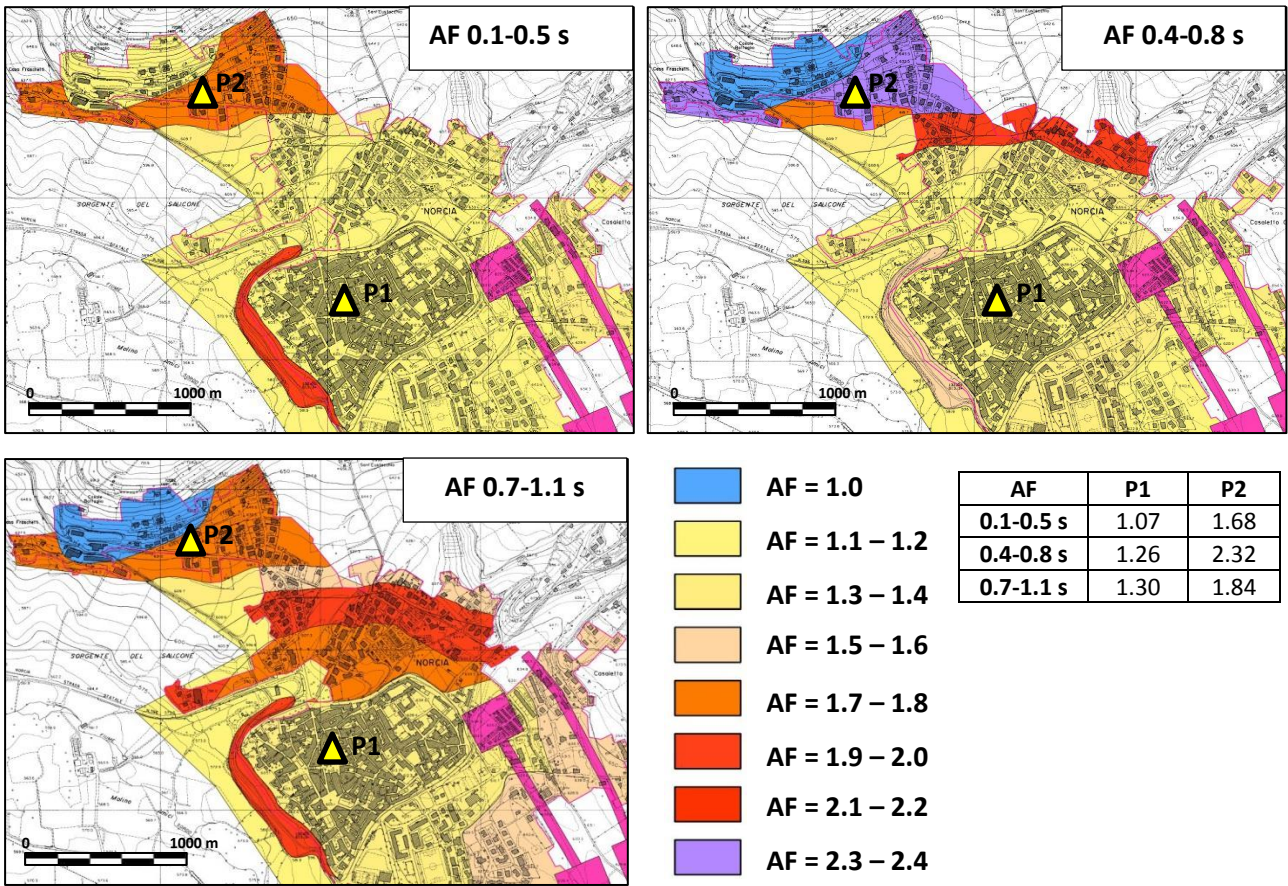


Figure 19. *Norcia site*: map of the amplification factors (FA)

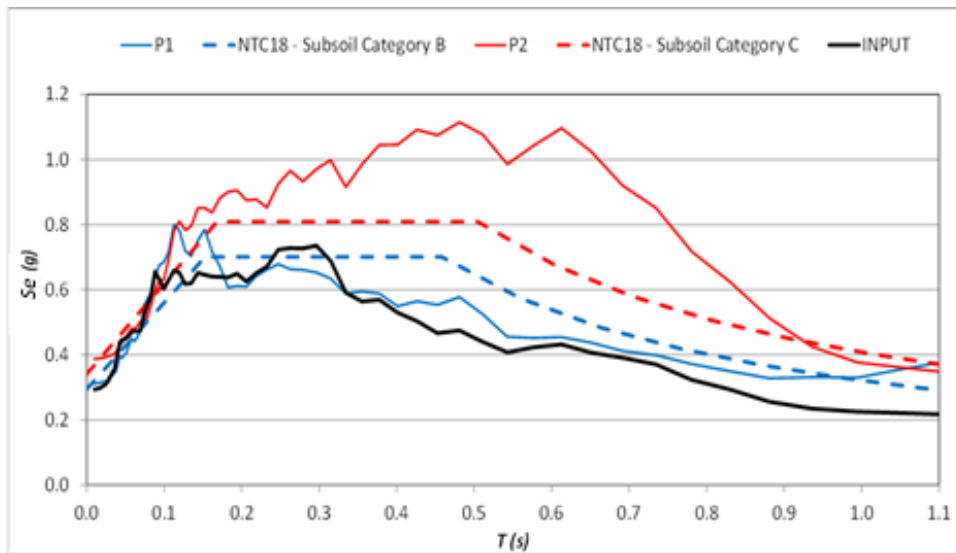


Figure 20. *Norcia site*: acceleration response spectra (black line: mean of the input motions; solid blue line: mean of the output at site P1; solid red line: mean of the output at site P2; dashed blue line: NTC18 spectra for subsoil Category B; dashed red line: NTC18 spectra for subsoil Category C).

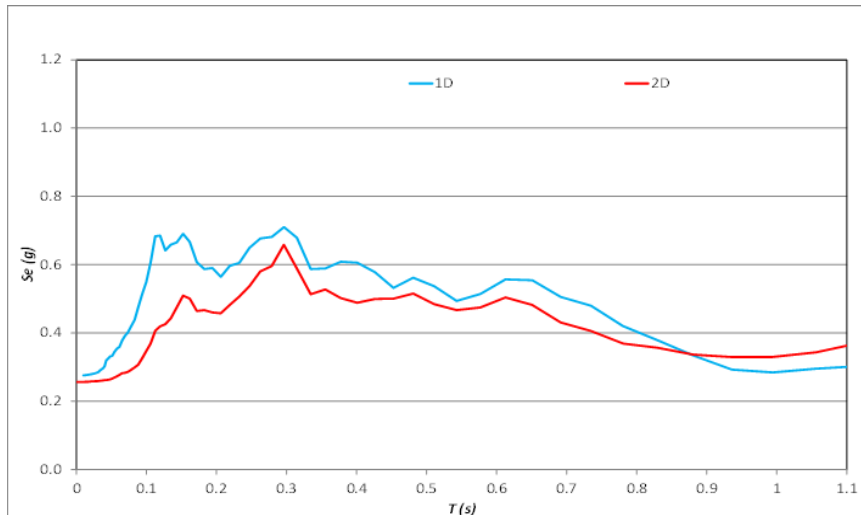


Figure 21. *Norcia site*: mean elastic response spectra obtained with 1D and 2D modelling at P1 site.

## 7. Discussion and conclusions

The site response analysis of the different sites presented in this study, characterized by different complex geological and geomorphological conditions, made it possible to highlight some considerations that could be applied for seismic microzonation studies in similar configurations. Relevant lessons are discussed in the following for the different morphological configurations analysed (ridge, slope and valley).

### Slope configuration

In Monte San Martino the ground motion amplification on the slope is mainly attributed to stratigraphic effects associated to soil cover resting on bedrock. These effects are significantly predominant with respect to 2D effects related to topography and the inclined geometry of the interface between bedrock and soil layers, with the exception at the edge of soil cover (V2). This result suggests that, for seismic microzonation in such morphological configurations, 1D analyses could be enough to provide reliable estimation of amplification factors, despite the presence of an inclined bedrock. A simplified approach to consider topographic/morphologic effects (i.e., the application of a topographic factor of 1.2 from technical code, see NTC2018 and Eurocode 8 2003) can be considered as conservative.

### Ridge configuration

The Montedinove case study highlighted the importance of seismic bedrock depth. Neglecting a shear wave velocity inversion below an upper stiff formation constituting the ridge (i.e. selecting the upper formation as seismic bedrock) results in a quite different response with respect to the analyses executed assigning the bedrock below the soft formation. Using this “deep bedrock” option causes a damping of medium-to-high frequencies and an increment of low-to-medium ones. Large scale investigations are therefore crucial in microzonation studies for the correct identification of seismic bedrock; this is usually achieved by an expert combined use of geological surveys and geophysical investigations.

The Arquata case has shown the coupling between topographic effects and stratigraphic effects associated with the presence of an upper weathered/jointed portion of the rockmass (“atypical topographic effects” according to Massa et al. 2014). In these contexts, the evaluation of site amplification is problematic (Pagliaroli et al., 2015). On the one hand, numerical codes do not generally allow a reliable representation of the subsoil complexity (e.g., discontinuous behavior of rock mass due to jointing); on the other hand, such materials are generally difficult or expensive to characterize with standard active geophysical techniques (i.e. MASW or in-hole tests). The case study has shown that the numerical model can be successfully calibrated by using H/V from noise measurements which provided encouraging results also in such complex configurations or, hopefully, using linear amplification functions obtained from recordings of a temporary network (i.e., by means of GIT technique). This choice may appear expensive but is a valid alternative in the case of microzonation in rock-mass regions. The recording of small amplitude events is not a substantial limitation because the rock mass behavior is essentially linear. Both ridge cases highlight the importance of 2D ridge resonance governing the seismic response for periods corresponding to wavelengths comparable with the base size of the relief. In this period range topographic effects are significant and exceed the simplified amplification factors proposed by technical codes.

### Valley configuration

In Capitignano, located close to the edge of a large valley constituted by an extensive fault damage zone, significant ground motion variations for distance of the order of 100-200 m are observed due to 2D effects probably related to the propagation of lateral surface waves generated at the edge interacting with direct waves. In the valley an aggravation factor of about 2 with respect to 1D prediction has been computed for periods higher than 1 s while in the fault damage zone, moderate 2D effects occur. The execution of 2D analyses is therefore mandatory for seismic microzonation studies in such context to properly estimate amplification factors in the valley infill, least within a few hundred from the edge. Large scale geological and geophysical investigations are necessary to define the buried morphology which strictly controls the amplification pattern (edge slope angles, presence of fault steps at depth,...).

Norcia is in the center of a large valley (aspect ratio 0.1) in which 2D effects can be neglected at least in the frequency range of interest. The geological and geotechnical characterization (i.e., the  $V_s$  profile) of the infill is crucial because the response is controlled by stratigraphic effects. In particular, the analyses have shown that the presence of an inversion of the S-wave velocity at the centre of the valley (site P1) strongly controls the response because a substantial amount of energy is trapped and dissipated within the soft layer, due to nonlinear soil behaviour. Like Montedinove case study, deep geophysical investigations are necessary to define the  $V_s$  profile at large depths. In-hole technique are generally too expensive while ESAC (i.e., 2D passive seismic arrays), successfully employed in Norcia, can provide useful information with acceptable costs.

### **Acknowledgement**

The project was carried out with the funding from the National Authorities in the context of "Interventi urgenti in favore delle popolazioni colpite dagli eventi sismici del 2016" (Urgent interventions for the populations affected by the 2016 earthquakes).

The Authors want to thank all the professional geologists who have collaborated on the execution of the whole project: Luca Domenico Venanti, Luciano Faralli, Nello Gasparri, Riccardo Piccioni (Norcia), Mirko Gattoni, Riccardo Maria Bistocchi, Stefano Bellaveglia (Arquata del Tronto), Alessandra Angelici (Montedinove), Stefano Cicora (Monte San Martino).

Thanks also to the "Centro per la Microzonazione Sismica e le sue Applicazioni" (CentroMS, <https://www.centromicrozonazioneismica.it/en/>) which coordinated the seismic microzonation project.

### **References**

Amanti M., Catalano S., Cavuoto G., Della Seta M., Di Naccio D., Esposito C., Fantozzi P.L., Mancini M., Mirabella F., Moscatelli M., Muraro C., Paolucci E., Peronace E., Pieruccini P., Pizzi A., Romagnoli G., Tallini M., Tortorici G. (2019) Geological model definition and engineering geology contribution to seismic microzonation. Bulletin of Earthquake Engineering (this issue).

Angelici A. (2018) Microzonazione Sismica di Livello 3 del Comune di Montedinove ai sensi dell'ordinanza del Commissario Straordinario n°24 registrata il 15 maggio 2017 al n°1065, Comune di Montedinove, Relazione illustrativa (in Italian).

Bard P.-Y., Bouchon M. (1985) The two-dimensional resonance of sediment-filled valleys. Bull Seismol Soc Am 75:519-541.

Bard P.-Y., Gariel J.-C. (1986) The seismic response of two-dimensional sedimentary deposits with large vertical velocity gradients. Bull. Seismol. Soc. Am. 76, 343-346.

Blumetti A.M. (1995) Neotectonic investigations and evidence of paleoseismicity in the epicentral area of the January-February 1703, central Italy, earthquakes, in: Serva L. and Slemmons D.B. (eds), Perspectives in paleosismology, Ass. of Eng. Geol., spec. publ., 6, 83-100.

Boncio P., Lavecchia G., Milana G., Rozzi B. (2004). Seismogenesis in Central Apennines, Italy: an integrated analysis of minor earthquake sequences and structural data in the Amatrice-Campotosto area. Annals of Geophysics, 47(6), 1723-1742.

Bramerini F., Campolunghi M.P., Castenetto S., Naso G., Scionti V. (2015) Microzonazione sismica, Standard di rappresentazione e archiviazione informatica (ver. 4.0b) DPC, pp. 122 [in Italian]. available at: [http://www.protezionecivile.gov.it/resources/cms/documents/StandardMS\\_4\\_0b.pdf](http://www.protezionecivile.gov.it/resources/cms/documents/StandardMS_4_0b.pdf).

- Centamore E., Cantalamessa G., Micarelli A., Potetti M., Berti D., Bigi S., Morelli C., Ridolfi M. (1991) Stratigrafia e analisi di facies dei depositi del Miocene e del Pliocene inferiore dell'avanfossamarchigiano-abruzzese e delle zone limitrofe. *Studi Geologici Camerti*, vol. spec. 1991/2, 125-131.
- Chiaraluce L., Di Stefano R., Tinti E., Scognamiglio L., Michele M., Casarotti E., Cattaneo M., De Gori P., Chiarabba C., Monachesi G., Lombardi A.M., Valoroso L., Latorre D., & Marzorati S. (2017) The 2016 Central Italy seismic sequence: a first look at the mainshocks, aftershocks and source models. *Seism. Res. Lett.*, 88 (3), 1-15, doi:10.1785/0220160221.
- Chiarini E., La Posta E., Cifelli F., D'Ambrogi C., Eulilli V., Ferri F., Marino M., Mattei M., Puzzilli L.M. (2014) A multidisciplinary approach to the study of the Montereale Basin (Central Apennines, Italy). *Rend. Fis. Acc. Lincei*, 25: 177, doi 10.1080/16445647.2016.1239229.
- Ciancimino A., Foti S., Alleanza G.A., Amoroso S., Bardotti R., Biondi G., Cascone E., Castelli F., D'Onofrio A., Lanzo G., Lentini V., Madiari C., Vessia G. (2019) Dynamic characterization of soils in Central Italy through laboratory testing. *Bulletin of Earthquake Engineering* (this issue).
- Civico R., Blumetti A.M., Chiarini E., Cinti F.M., La Posta E., Papasodaro F., Sapia V., Baldo M., Lollino G., Pantosti D. (2016) Active traces of the Capitignano and San Giovanni faults (Abruzzi Apennines, Italy). *Journal of Maps*, doi 10.1080/16445647.2016.1239229.
- CNR-IGAG (2017) Rapporto completo – versione 1, analisi dei dati sismologici esistenti ai fini della MS di livello 3, stima dell'amplificazione sismica e degli spettri di risposta specifici di sito,. Prodotto 4.2, pp. 203 [in Italian].
- D'Agostino N., Giuliani R., Mattone M., Bonci L. (2001) Active crustal extension in the central Apennines (Italy) inferred from GPS measurements in the interval 1994–1999, *Geophys. Res. Lett.* 28, 2121-2124.
- Caielli G., De Franco R., Di Fiore V., Albarello D., Amanti M., et al. (2019) Extensive geophysical prospecting for seismic microzonation. *Bulletin of Earthquake Engineering* (this issue).
- Cosentino D., Asti R., Nocentini M., Gliozzi E., Kotsakis T., Mattei M., Esu D., Spadi M., Tallini M., Cifelli F., Pennacchioni M., Cavuoto G., Di Fiore V. (2017) New insights into the onset and evolution of the central Apennine extensional intermontane basins on the tectonically active L'Aquila Basin (central Italy). *GSA Bulletin*, 129 (9-10), 1314-1336, doi: 10.1130/B31679.1.
- Darendeli M.B. (2001) Development of a new family of normalized modulus reduction and material damping curves. PhD thesis, The University of Texas at Austin, pp. 394, available at: <https://repositories.lib.utexas.edu/bitstream/handle/2152/10396/darendelimb016.pdf>
- Di Buccio F., Aprile V., Pagliaroli A., Di Domenico A., Pizzi A. (2017) Valutazione preliminare della risposta sismica locale del bacino di Sulmona. *Atti Incontro Annuale dei Ricercatori di Geotecnica IARG2017*, 2017, July 5-7, Matera (Italy), Publisher Universosud, ISBN: 978-88-99432-30-0 (in italian).
- Eurocode 8 (2003) Design provisions for earthquake resistance of structures — Part 5: foundations, retaining structures and geotechnical aspects, ENV 1998–5, CEN European Committee for Standardisation, Brussels.
- Galadini F., Messina P., Giaccio B., Sposato A. (2003) Early uplift history of the Abruzzi Apennines (central Italy): available geomorphological constraints, *Quaternary International* 101/102, 125-135.
- Galadini F., Galli P. (2000) Active tectonics in the Central Apennines (Italy) - Input data for seismic hazard assessment, *Nat. Hazards* 22, 225-270.
- Galli P., Galadini F., Calzoni F. (2005) Surface faulting in Norcia (central Italy): a “paleoseismological perspective”, *Tectonophysics* 403, 117–130.
- Hashash Y., Musgrove M., Harmon J., Groholski D., Phillips C., Park D. (2016) DEEPSOIL 6.1, User Manual. Urbana, IL: Board of Trustees of University of Illinois at Urbana-Champaign.
- Hudson M., Idriss I., Beikae M. (1994) User's Manual for QUAD4M. Center for Geotechnical Modeling, Department of Civil & Environmental Engineering, University of California, Davis, California.



ISPRA (2017) Attività propedeutiche alla Microzonazione Sismica nell'area del comune di Arquata del Tronto (AP). Report (in Italian)

Koopman A. (1983) Geological Map of the Eastern edge of the Umbria Marche Apennines (Umbria thrust zone) and Laga Mountains area. *Geologica Ultraiectina Mededelingen van het Instituut voor Aardwetenschappen det Rijksuniversiteit te Utrecht No. 30 Detachment tectonics in the Central Apennines, Italy.*

Kottke A.R., Rathje E.M. (2008) Technical Manual for Strata, PEER Report 2008/10, Pacific Earthquake Engineering Research Center College of Engineering, University of California, Berkeley, available at: [http://peer.berkeley.edu/publications/peer\\_reports/reports\\_2008/web\\_PEER810\\_KOTTKE\\_Rathje.pdf](http://peer.berkeley.edu/publications/peer_reports/reports_2008/web_PEER810_KOTTKE_Rathje.pdf).

Kuhlemeyer R.L., Lysmer J. (1973) Finite element method accuracy for wave propagation problems, *J. of the Soil Mechanics and Foundations Div.*, 99(SM5), 421-427.

Lanzo G., Pagliaroli A., D'Elia B. (2003) Numerical study on the frequency-dependent viscous damping in dynamic response analyses of ground. In Latini & Brebbia (eds), *Earthquake Resistant Engineering Structures IV*, WIT Press, Southampton, Boston, pp. 315-324.

Luzi L., Hailemichael S., Bindi D., Pacor F., Mele F., Sabetta F. (2008) ITACA (Italian ACcelerometric Archive): a web portal for the dissemination of Italian strong-motion data. *Seismological Research Letters*, 79(5), 716-722.

Luzi L., Pacor F., Felicetta C., Puglia R., Lanzano G., D'Amico M. (2019a) 2016-2017 Central Italy seismic sequence: strong-motion data, seismic hazard and design earthquake for the seismic microzonation of Central Italy. *Bulletin of Earthquake Engineering* (this issue).

Luzi L., Massa M., Puglia R., D'Amico M. (2019b) Site effects observed in the Norcia intermountain basin (Central Italy): results after twenty-year monitoring. *Bulletin of Earthquake Engineering*, 17(1), 97-118.

Macerola L. (2017) Caratterizzazione sismica di sito e risposta sismica locale tramite simulazioni 1D e 2D di casi in studio nel comprensorio aquilano. [Seismic site characterization and local seismic response by means of 1D and 2D simulations of L'Aquila case-studies] (in Italian) PhD thesis, L'Aquila University, pp. 229.

Marini M., Milli S., Ravnås R., Moscatelli M. (2015) A comparative study of confined vs. semi-confined turbidite lobes from the Lower Messinian Laga Basin Central Apennines, Italy: implications for assessment of reservoir architecture. *Marine and Petroleum Geology* 63, 142-165.

Massa M., Barani S., Lovati S. (2014) Overview of topographic effects based on experimental observations: meaning, causes and possible interpretations. *Geophys J Int.* doi:10.1093/gji/ggt341

NTC2018 D.M. 17/01/2018. Aggiornamento delle «Norme tecniche per le costruzioni». *Gazzetta Ufficiale*, n.42 del 20/02/2018 – supplemento ordinario n.8 (in Italian).

Pagliaroli A., Lanzo G., D'Elia B. (2011) Numerical evaluation of topographic effects at the Nicastro ridge in Southern Italy. *Journal of Earthquake Engineering*, 15(3), 404-432.

Pagliaroli A., Avalle A., Falcucci E., Gori S., Galadini F. (2015) Numerical and experimental evaluation of site effects at ridges characterized by complex geological setting. *Bulletin of Earthquake Engineering*, 13:2841-2865.

Pagliaroli A. (2018) Key issues in Seismic Microzonation studies: lessons from recent experiences in Italy. *Rivista Italiana di Geotecnica - Italian Geotechnical Journal*, n. 1/2018, pp. 5-48, DOI: 10.19199/2018.1.0557-1405.05.

Paolucci R. (2002) Amplification of earthquake ground motion by steep topographic irregularities. *Earthquake Engineering and Structural Dynamics* 31, 1831-1853.

Pierantoni P., Deiana G., Galdenzi S. (2013) Stratigraphic and structural features of the Sibillini Mountains (Umbria-Marche Apennines, Italy). *Ital. J. Geosci. (Boll. Soc. Geol. It.)*, 132 (3), 497-520. doi: 10.3301/IJG.2013.08.

Pizzi A., & Galadini, F. (2009) Pre-existing cross-structures and active fault segmentation in the northern-central Apennines (Italy). *Tectonophysics*, 476, 304-319. <https://doi.org/10.1016/j.tecto.2009.03.018>.

Priolo E., Pacor F., Spallarossa D., Milana G., Laurenzano G., Romano M.A., Felicetta C., Hailemichael S., Cara F., Di Giulio G., Ferretti G., Barnaba C., Lanzano G., D'Amico M., Puglia R., Scafidi D., Barani S., De Ferrari R., Cultrera G. (2018) Seismological analyses aimed at seismic microzonation of the 138 municipalities damaged by the 2016-2017 seismic sequence in Central Italy. *Bulletin of Earthquake Engineering* (present issue).

Ramberg W., Osgood WR., (1943) Description of stress–strain curves by three parameters. Technical Note No. 902, National Advisory Committee For Aeronautics, Washington DC.

REGIONE MARCHE (2001) Progetti CARG e Obiettivo 5B. P.F. Informazioni Territoriali. Available at: <http://www.regione.marche.it/Regione-Utile/Paesaggio-Territorio-Urbanistica/Cartografia/Repertorio/Cartageologicaregionale10000>

Riga E., Makra K., Pitolakis K., (2016) Aggravation factors for seismic response of sedimentary basins: a code-oriented parametric study. *Soil Dyn. Earthq. Eng.* 91, 116–132.

Rollins K.M., Evans M.D., Diehl N.B., Daily III W.D. (1998) Shear modulus and damping relationships for gravels. *Journal of Geotechnical and Geoenvironmental Engineering*, 124(5), 396-405.

Seed HB., Idriss IM. (1970) Soil moduli and damping factors for dynamic response analyses, Report no. EERC 70-10. Earthquake Engineering Research Center, University of California, Berkeley, California.

STACEC srl (2017) LSR 2d (Local Seismic Response 2d), <http://www.stacec.com>.

Tallini M., Berti D., Chiarini E., D'Andrea V., Durante F., Fernando F., La Posta E., Macerola L., Nocentini M., Palucci D., Puzzilli L.M., Roma M., Silvestri S. (2017) Relazione tecnico-scientifica finale - Macroarea Capitignano - Santa Lucia. Accordo tra CNR IGAG e DPC per le attività di supporto al Dipartimento della Protezione Civile per la fase emergenziale a seguito del terremoto 2016-2017 del Centro Italia, Prot. CNR IGAG n°0001484 del 17/05/2017 (in Italian).

Vucetic M., Dobry R. (1991) Effect of soil plasticity on cyclic response. *Journal of geotechnical engineering*, 117(1), 89-107.

Working Group ICMS (2008) Indirizzi e criteri per la microzonazione sismica – Guidelines for seismic microzonation. Conferenza delle Regioni e delle Province Autonome-Dipartimento della Protezione Civile. English version available at [http://www.protezionecivile.gov.it/httpdocs/cms/attach\\_extra/GuidelinesForSeismicMicrozonation.pdf](http://www.protezionecivile.gov.it/httpdocs/cms/attach_extra/GuidelinesForSeismicMicrozonation.pdf).